Project 019 Development of Aviation Air Quality Tools for Airport-Specific Impact Assessment: Air Quality Modeling

University of North Carolina at Chapel Hill

Project Lead Investigator

Saravanan Arunachalam, PhD
Research Professor
Institute for the Environment
University of North Carolina at Chapel Hill
123 W. Franklin St., Suite 330B
Chapel Hill, NC 27516
919-966-2126
sarav@email.unc.edu

University Participants

University of North Carolina at Chapel Hill (UNC Chapel Hill)

- P.I.: Saravanan Arunachalam, Research Professor and Deputy Director
- FAA Award Number: 13-C-AJFE-UNC Amendments 1–21
- Period of Performance: October 1, 2024, to September 30, 2026
- Tasks:
  1. Develop and evaluate a new dispersion model for aircraft sources
  2. Develop and evaluate a multiscale Weather Research and Forecasting (WRF)-Sparse Matrix Operator Kernel Emissions (SMOKE)-Community Multiscale Air Quality (CMAQ) model application for Boston Logan International Airport (BOS) focused on ultrafine particles (UFP)
  3. Implement volatile particulate matter (PM) plume-scale modeling into a CMAQ application

Project Funding Level

The Federal Aviation Administration (FAA) provided $650,000 in funding. The Barr Foundation provided matching cost-share via the Harvard Center for Climate, Health, and the Global Environment.

Investigation Team

Prof. Saravanan Arunachalam, P.I., UNC Chapel Hill Institute for the Environment
Dr. Gavendra Pandey, Air Quality Dispersion Modeler, UNC Chapel Hill Institute for the Environment
Hyeongseok “Darby” Kim, Graduate Student, UNC Chapel Hill Institute for the Environment
Brian Naess, Geographic Information Systems Specialist, UNC Chapel Hill Institute for the Environment
Dr. Huy Tran, Air Quality Modeler, UNC Chapel Hill Institute for the Environment
Rachel Snead, Aircraft Emissions Modeler, UNC Chapel Hill Institute for the Environment
Dr. Akula Venkatram, Consultant, University of California at Riverside

Project Overview

Aviation is predicted to grow steadily in upcoming years (Boeing, 2010); thus, a variety of aviation environmental policies will be required to meet emission reduction goals in aviation-related air quality and health impacts. Tools are needed to rapidly assess the implications of alternative policies for an evolving population and atmosphere. In the context of the International Civil Aviation Organization’s (ICAO) Committee on Aviation Environmental Protection, additional approaches are required to determine the implications of global aviation emissions.

The overall objective of this project is to develop a new aircraft-specific dispersion model and continue the development and implementation of tools, both domestically and internationally, to allow for an assessment of year-to-year changes in

significant health outcomes. These tools must be acceptable to the FAA (in the context of Destination 2025) and/or other decision makers. More importantly, this new model must have the capability to address the 1-hour form of the nitrogen dioxide (NO_2) National Ambient Air Quality Standard (NAAQS) in the United States (U.S.), as well as to support National Environmental Policy Act (NEPA) and/or NAAQS analyses that may be needed by airports. The developed methods must also rapidly provide output to support a variety of "what if" analyses and other investigations. While the tools for use within and outside the U.S. need not be identical, several goals are desirable for both cases:

- Enable the assessment of premature mortality and morbidity risks due to aviation-attributable PM having a diameter up to 2.5 μm ($PM_{2.5}$), ozone (O_3), and other pollutants known to exert significant health impacts.
- Capture airport-specific health impacts at regional and local scales.
- Account for the impact of landing/take-off (LTO) versus non-LTO emissions, including a separation of effects.
- Allow for an assessment of a wide range of aircraft emission scenarios, including differential growth rates and emission indices.
- Account for changes in non-aviation emissions.
- Allow for assessments of sensitivity to meteorology.
- Provide domestic and global results.
- Include quantified uncertainties and differences with respect to U.S. Environmental Protection Agency (EPA) practices, which are to be minimized when scientifically appropriate.
- Be computationally efficient, such that tools can be used in time-sensitive rapid turnaround contexts and for uncertainty quantification.

During this period of performance, the team at the University of North Carolina at Chapel Hill Institute for the Environment (UNC-IE) performed work on Tasks 1–3.

Task 1 - Develop and Evaluate a New Dispersion Model for Aircraft Sources

University of North Carolina at Chapel Hill

Objectives

The FAA's Aviation Environmental Design Tool (AEDT) is currently coupled with the American Meteorological Society/EPA Regulatory Model (AERMOD[1]) dispersion model for modeling aircraft sources and is the required regulatory model in the U.S. for modeling airport-level aircraft operations during LTO cycles.

Recent studies have shown several limitations in the use of AERMOD for modeling aircraft sources. The Airport Modeling Advisory Committee developed a series of recommendations in 2011 to improve jet exhaust modeling. Since then, the Airport Cooperative Research Program (ACRP) Project 02-08 developed guidance for airport operators on conducting measurements and modeling of air quality at airports, published in ACRP Report 71 (Kim et al., 2012), with a measurement and modeling study conducted at Dulles International Airport (IAD). Subsequently, the ACRP Project 02-58 developed the final ACRP Report 171 (Arunachalam, Valencia, et al., 2017) providing dispersion modeling guidance for airport operators for local air quality and health. This study applied four different models—AERMOD, CALPUFF,[2] Second Order Closure Integrated Puff Model with Chemistry (SCICHEM), and the United Kingdom's Atmospheric Dispersion Modeling System for Airports (ADMS-Airport)—for the Los Angeles International Airport (LAX) and compared model predictions with high-resolution measurements taken during the LAX Air Quality Source Apportionment Study (AQSAS). Each of these reports identified several limitations with AERMOD and developed a series of recommendations for improving dispersion modeling of aircraft emissions for airport-level air quality.

In 2017, UNC-IE developed the C-AIRPORT dispersion model for application to LAX (Arunachalam, Isakov, et al., 2017). Initially, C-AIRPORT was designed to be part of the C-TOOLS series of community-scale, web-based modeling systems. The objective of C-TOOLS was to create a web-based interface for modeling multiple source types for short-term or long-term pollutant concentration averages and for analyzing various "what if" scenarios to assess changes in air quality at local scales due to changes in inputs. C-AIRPORT used a line source-based approach to model aircraft sources, based upon the

[1] AERMOD is a steady-state plume model that incorporates air dispersion based on planetary boundary layer turbulence structure and scaling concepts.
[2] CALPUFF is an advanced non-steady state air quality dispersion model maintained and distributed by Lake Environmental.

C-LINE modeling system (Barzyk et al., 2015), and a preliminary evaluation of the algorithms against LAX AQSAS was conducted. Preliminary results at LAX core sites showed that nitrogen oxide (NO_x) model estimates from all sources were generally comparable to observations except for slight overpredictions, given lack of plume rise. However, overall, aircraft contribution seems low compared to other sources. Further, investigation is needed to continue the evaluation of C-AIRPORT.

Under the previous year's funding, UNC-IE completed development of a modeling framework that addresses known limitations from the above tasks and proposed a viable and suitable approach for modeling pollutants from aircraft sources. The primary objective of this plan was to demonstrate that a robust, improved pollutant dispersion model for aircraft can be developed for U.S. regulatory compliance purposes. The proposed new model will disperse pollutants from aircraft sources in a more technically and scientifically advanced manner (compared with current AERMOD capabilities), with the ultimate goal of becoming a potential U.S. regulatory compliance tool, based on future discussions with FAA and EPA. This plan will include an itemized list of known limitations along with a corresponding proposed developmental approach and recommendations for addressing the limitations.

As part of the proposed ASCENT research under this task, we will continue to implement the plan with a specific focus on four broad areas. This report provides a very high-level summary here, because the specifics of this implementation have been described in previous documents and reports that were independently developed earlier.

Our approach is to ensure that the new model will be "robust" and based on the state of science on physical and chemical processes and associated algorithms.

Source Characterization
Existing approaches in AEDT/AERMOD treat aircraft sources as an area source segment. In the ongoing work, our team is developing two aircraft dispersion models. The first is a simple analytical steady-state plume model, referred to as the aircraft dispersion model (ADM), while the second is a grid-based unsteady-state model, referred to as GADM. In ADM, surface-level aircraft sources are treated as area sources, whereas airborne sources are modeled as pseudo-volume sources. Conversely, in GADM, all aircraft sources are treated as volume sources. To generate input emissions for these models, our team has developed an emission processor called AEDT2ADM. This processor utilizes high-resolution aircraft movement datasets from the AEDT. AEDT2ADM is continuously adapted to enhance its usability for other existing models too, such as AERMOD.

Physical Processes
In previous years, our team already developed an aircraft plume-rise algorithm for the area/volume sources framework (Pandey et al., 2023) by assuming that the different types of aircraft contributing to emissions in any one of the area/volume sources can be represented by a "typical" aircraft whose characteristics computed through a weighted average of the characteristics of aircraft that pass through the area/volume source. Emissions from an aircraft are treated as line thermals that have horizontal momentum and buoyancy. This algorithm is used in ADM and GADM.

In addition to plume rise, our team will go beyond the initial implementation developed during the previous year, with a new focus on the following:

a. Treatment of dispersion under low wind conditions and assessment of effects of atmospheric stability
b. Treatment of dry and wet deposition
c. Incorporation of aircraft downwash effects
d. Treatment of complex terrain and building downwash

Chemical Processes
Our team will go beyond the initial implementation of the previous year, with a new focus on the following:

a. The 1-hr form of the NO_2 NAAQS. The 1-hour form of the NO_2 NAAQS is a critical issue for air quality around U.S. airports, with several modeling studies showing overestimates compared with observations. It is important that the new model performs adequately to capture this short-term form of the NO_2 NAAQS.
b. A new detailed chemical mechanism for NO_2 including the generic reaction set (Valencia et al., 2018; Venkatram et al., 1994) or other components.
c. Version of the aerosol treatment as included in the CMAQ and SCICHEM and described by Chowdhury et al. (2015).

Model Evaluation

a. Ongoing model evaluation has involved evaluating model predictions using only measurements from the LAX AQSAS for winter 2012. Our team will now consider developing and testing the model for other case studies, including the following:
   1. LAX AQSAS for Summer 2012
   2. One of three airports (Copenhagen, Madrid, and Zurich) with measurements being undertaken as part of the European Union (EU) Assessing aviation emission Impact on local Air quality at airports: Towards Regulation (AVIATOR) project, a new measurement-modeling study called AVIATOR undertaken in Europe through funding from the EU.[3]
      i) Our team will rely on the AVIATOR team to provide emission inventories for the chosen airport. If emission inventories are not directly available for use, we will obtain airport operations data for the campaign period and develop an inventory using the AEDT.
   3. New measurements from the ASCENT Project 018 investigators at BOS and IAD
      i) This is a new collaboration that will help focus on both designing the monitoring campaign to assist in obtaining valuable data for characterizing the impact of aircraft emissions on air quality and developing the ADM, as well as in source attribution of the measured fields to the aircraft or other source types.

b. Model evaluation will focus on the model's ability to capture the behavior of the plume related to aircraft sources during LTO cycles at an airport, while comparing with available observations and identifying strengths and weaknesses compared with another existing model.

c. In collaborating with Boston University (BU), we will rely on BU to perform appropriate cleanup and quality assurance/control of observation data before using these data in our model evaluation routines. Our team will also work closely with BU to ensure appropriate and careful interpretation of the data. UNC-IE and BU have collaborated extensively on similar projects in the past, and we expect to obtain a robust model measurement and modeling assessment from the BOS study.

Research Approach

1. Source Characterization

Aircraft LTO emissions contribute to surface air quality in and around an airport. Dispersion modeling helps to quantify the effects of aircraft emissions on surface air quality. We started working on two tasks: (1) understand the effects of airborne aircraft emissions on surface air quality and (2) understand the effects of varying numbers of sources in dispersion modeling. Although there are many studies on the effects of aircraft surface emissions on surface air quality, the effects of airborne emissions on surface air quality in dispersion modeling remain poorly understood. To accomplish both tasks, UNC-IE updated the Python®-based emissions processor AEDT2ADM (developed earlier for ADM) that generates the required input files for the AERMOD dispersion model. We hope to complete these tasks in the next performance period.

2. Physical Processes

2.1 Development and Implementation of an Aircraft Plume Rise Algorithm in AERMOD

Aircraft emissions, especially during the LTO cycle, play a significant role in degrading the air quality in and around airports. Unlike stationary sources, these emissions are characterized by high forward momentum and thermal buoyancy due to jet engine exhaust, which affects how pollutants disperse in the atmosphere. Neglecting these characteristics in a dispersion model frequently results in an overprediction of ground-level pollutant concentrations near airports. Recently, Pandey et al. (2023) implemented this unique but complex characteristic of aircraft plume dynamics in the EPA's regulatory model AERMOD, and further in Pandey et al. (2024), extensively evaluated this algorithm using observations from the LAX AQSAS, conducted at LAX in 2012. They found that AERMOD performs significantly better after the inclusion of aircraft-specific plume rise. This algorithm was subsequently promulgated by EPA as an ALPHA option in AERMOD version 23132. It is publicly available to use as a research option (ALPHA) within the recent version of AERMOD 24142. Here, we presented the updates on this aircraft plume rise algorithm and its evaluation against the LAX AQSAS 2012 and Boston 2024 studies.

2.1.1 Aircraft Plume Rise Methodology within AERMOD

The existing aircraft plume rise algorithm within AERMODv24142 has a simplified assumption of plume dynamics; it takes all the emissions from all different types of aircraft in any one of the fixed area sources and represents them as a "typical" aircraft. The characteristics of this typical aircraft are a weighted average of all actual aircraft that pass through that area source.

[3] https://aviatorproject.eu/

® Python is a registered trademark of Python Software Foundation, Beaverton, Oregon.

According to this existing algorithm, an exhaust plume behaves as follows:

a. It starts as a line of hot air driven by the aircraft's forward momentum. This initial thrust causes the plume to expand horizontally as it travels away from the aircraft.
b. Once the plume slows down to the speed of the surrounding wind, buoyancy takes over.
c. The plume stops rising when it either hits a layer of stable air and loses its lift or when atmospheric turbulence becomes strong enough to break it apart.

The horizontal momentum and the buoyancy of the line thermal associated with jet aircraft emissions are related to aircraft engine characteristics: thrust, fuel burn rate, aircraft velocity, air-fuel ratio, rated power, and engine bypass ratio. Details of the formulation are provided in Pandey et al. (2023).

Overall, this existing algorithm separately calculates the plume rise generated because of horizontal momentum and buoyancy and combines both of them. Due to this, it is unable to accurately capture the characteristics of plume dynamics that are governed by plume velocity causing the algorithm to calculate significantly high plume rise values. To overcome these issues, we modified this into a new, aircraft-specific plume rise algorithm within AERMOD.

2.1.1.1 Reformulated Aircraft Plume Rise Algorithm

From the incompleteness in the existing aircraft plume rise algorithm, we have updated it and describe these updates below. It builds upon our improved understanding of plume rise of emissions from aircraft sources and could be readily incorporated into AERMOD. Here, we have given brief information about the updated aircraft-specific plume rise algorithm.

The calculations of heat rejection, exhaust temperature, and buoyancy flux are identical to the existing algorithm. However, we updated the interaction of the buoyancy-induced plume with the horizontal momentum plume using the following equations:

Plume rise due to buoyancy, z_p, is governed by:

$$\frac{dz_p}{dt} = w_p, \qquad \text{(Eq. 1)}$$

where w_p is the buoyancy-induced vertical velocity given by combining the momentum and energy balances on the plume element,

$$\frac{d}{dt}\left(r^2 w_p\right) = F_o. \qquad \text{(Eq. 2)}$$

The radius of the plume r grows through the combined effect of shear between the rising plume and the surrounding air and atmospheric turbulence:

$$\frac{dr}{dt} = \beta w_p + \sigma_w, \qquad \text{(Eq. 3)}$$

where $\beta = 0.6$ is an entrainment constant, and σ_w is the standard deviation of the vertical velocity fluctuations of the surrounding atmosphere.

Solving the above equations results in the final combined plume rise.

Note that the radius of the plume grows in response to the effects of both horizontal motions caused by exhaust momentum and the vertical motion caused by buoyancy.

2.1.1.2 Computation of Plume Rise Magnitudes

We have compared the plume-rise magnitudes from both algorithms— the publicly available AERMOD version 24142 (Plume Rise_Old) and the updated one presented here (Plume Rise_New)— for all LTO modes. For this, we calculated final plume-rise values up to 1000 m downwind of the source by considering all possible combinations of engine parameters (fuel burn rate, thrust, by-pass ratio, and rated power [for shaft-based engines]) for each LTO mode, over a single stable meteorological hour (wind speed, 3.5 m/s; temperature, 298.15 K; surface roughness length, 0.03 m; Monin-Obukhov length, 100 m; surface friction velocity, 0.5 m/s; and mixing height, 200 m).

New plume rise values are significantly lower than old plume rise values at each LTO mode (Figure 1). These were also consistent with the light detection and ranging (LiDAR) experiment measured values by Wayson et al. (2008).

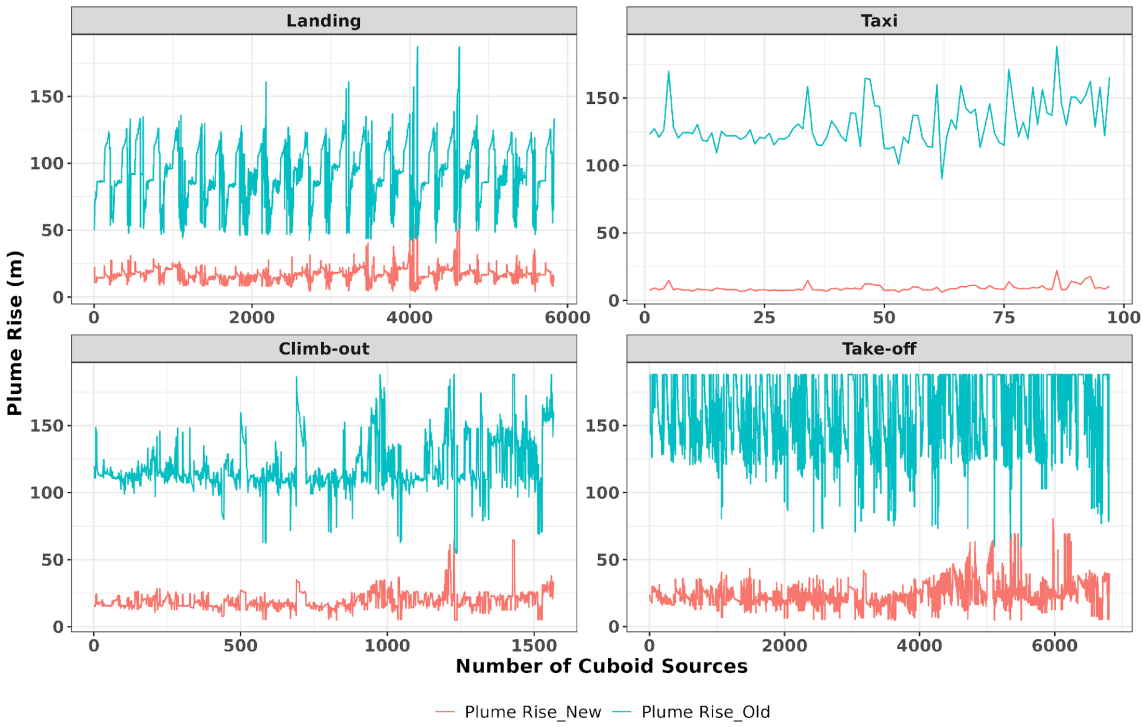

Figure 1. Comparison of old and new plume rise magnitudes for a single stable meteorological hour.

2.1.1.3 Step-Size Sensitivity

We have performed a sensitivity analysis based on the variation in step-size, Δx, by calculating the time taken by AERMOD using the new plume rise algorithm for a one-day LAX Summer 2012 study. In Table 1, from the old to new plume-rise (50 m step size) algorithm in AERMOD for one day, the runtime increases almost three times. All runs were performed on the UNC High Performance Computer (HPC) Longleaf server.

Table 1. AERMOD runtime comparison between old and new plume-rise algorithms. AQSAS: Air Quality Source Apportionment Study, HPC: high performance computer, LAX: Los Angeles International Airport, UNC: University of North Carolina.

Plume Rise Algorithm	Step Size (m)	UNC HPC Longleaf (AMDEPYC7702 x86_64 processor)	Run Time (hh:mm:ss)	Data Period (LAX AQSAS Summer 2012)
Old	NA	C1306ie01	00:14:50	One day
New	1	C1306ie01	23:26:12	One day
New	10	C1306ie01	02:35:41	One day
New	20	C1306ie01	01:25:33	One day
New	40	C1306ie01	00:50:16	One day
New	50	C1306ie01	00:43:18	One day

2.1.2 Case Study Applications

Here, we evaluated AERMOD with and without the aircraft-specific plume rise (old and new) options for the LAX AQSAS for 2012 and BOS Field Study for 2024.

2.1.2.1 Los Angeles International Airport Study

2.1.2.1.1 Site Description

To evaluate the air quality impact of LAX, a major global travel hub, the LAX AQSAS was conducted in 2012 (Figure 2). This study involved two intensive six-week monitoring campaigns during the winter and summer seasons, measuring pollutants like NO_x and sulfur dioxide (SO_2) at several locations in and around the airport. The main focus of this field study was at four "core" sites: AQ, CN, CS, and CE (Tetra Tech, 2013). The details of this study can be found in several studies (Arunachalam, Valencia, et al., 2017; Pandey et al., 2024, 2022).

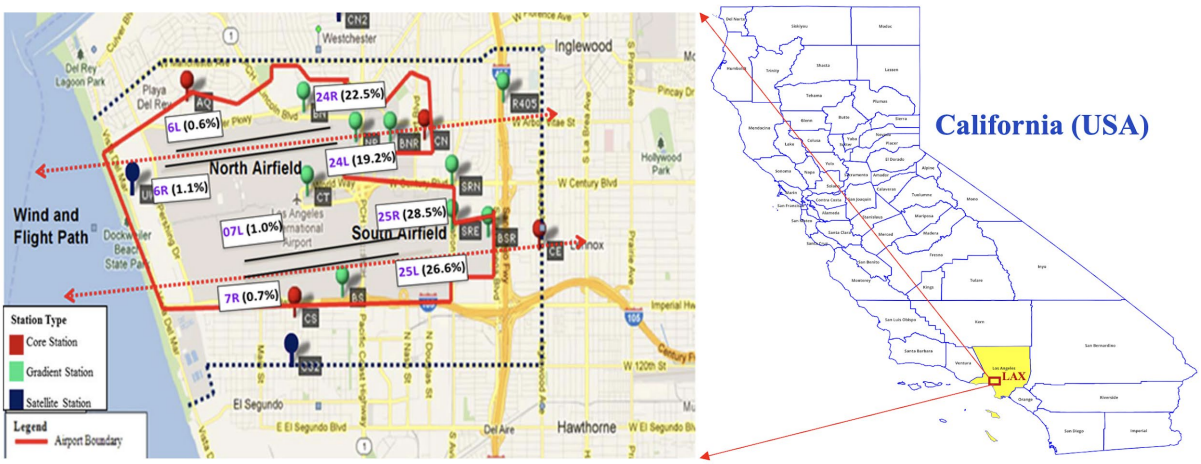

Figure 2. Locations of core, gradient, and satellite monitoring sites at Los Angeles International Airport (LAX). The red rectangle on the right surrounds Los Angeles County, containing the LAX airport, shown in greater detail on the inset map on the left. Adapted from ACRP Report 179 (Arunachalam, Valencia, et al., 2017).

2.1.2.1.2 Meteorological Data Input

The meteorological data for the AERMOD model were created using the AERMET[4] processor. In AERMET, as an input, surface observations from LAX airport, upper air data from a station in San Diego, California, and 1-min weather data from LAX were utilized. Further details on how the meteorological input files were created have been documented in several studies (Arunachalam, Valencia, et al., 2017; Pandey et al., 2024, 2022).

However, Pandey et al. (2022) identified a key limitation with the standard AERMET output: it doesn't fully characterize the heterogeneous/complex behavior of the turbulent internal boundary layer (IBL) that forms, especially on the shoreline at coastal sites. When cool ocean air blows over the warmer land of the airport, it creates an IBL. This layer enhances more mixing and dispersion of pollutants than AERMET would normally predict under stable conditions. To address this, Pandey et al. (2022) modified the meteorological data generated by AERMET.

2.1.2.1.3 Observation Data

A detailed analysis of observed SO_2 and NO_x concentrations and an explanation of potential contributions from aircraft activity during LTO operations are given in Pandey et al. (2024).

[4] AERMET is a meteorological data preprocessor for AERMOD. AERMET processes commercially available or custom on-site met data and creates two files: a surface data file and a profile data file.

2.1.2.1.4 Emission Data

Aircraft emissions of SO_2 and NO_x were calculated using the FAA's AEDT model, which models all the LTO models as distinct area sources of varying sizes. Non-aircraft emissions, which include sources like the nearby Chevron® refinery, road traffic, parking lots, and marine vessels, were taken from the emissions inventory generated during the LAX AQSAS 2012 study. A detailed discussion of the emissions inventory can be found in several studies (Arunachalam, Valencia, et al., 2017; Pandey et al., 2024, 2022).

We utilized both seasons' SO_2 and NO_x concentrations data to evaluate the aircraft-specific plume rise algorithms. However, here we have presented only the summer season results.

2.1.2.2 Boston Logan International Airport Study

To assess the robustness of the plume rise algorithm, we evaluated AERMOD using another dataset from the BOS Field Study. It was conducted by BU ASCENT Project 018 teams in the spring/summer and winter seasons of 2024. We received NO_x and SO_2 observation data from both monitoring periods, and we have extensively analyzed the dataset at UNC-IE. Here, we present the 2024 spring/summer season results, as we currently only have emissions for aircraft and non-aircraft sources for the spring/summer period. Based on the aircraft emissions inventory for the spring/summer of 2024, we have extracted the observation data for March 31 to July 31, 2024, to compare against the model. The results for this period are presented below.

2.1.2.2.1 Site Description

BOS is one of the main airports in the U.S. The BOS 2024 study involved extensive four-month (123 days) monitoring campaigns during the 2024 spring/summer season of 2024 (March 31 to July 31, 2024), measuring pollutants like NO_x and SO_2 at several locations around the airport. In the study, NO_x measurements were recorded at three locations: Revere (approximately 2.3 km from the start of runway 04R/22L and 2.4 km from the start of runway 04L/22R), Saratoga (approximately 0.7 km from the start of runway 04R/22L and 0.8 km from the start of runway 04L/22R), and Evans (approximately 1.8 km from the start of 14/32 runway), whereas SO_2 measurements were captured at only the Saratoga site (Figure 3). Out of the 123-day monitoring period, NO_x measurements were available for 49 days at Revere, 53 days at Saratoga, and 12 days at Evans (Figure 4). For SO_2, 91 days of data were available (Figure 4, Table 2).

Here, model estimates were compared with 1-hr averaged SO_2 and NO_x concentrations measurements made at all sites for the spring/summer season at BOS.

® Chevron is a registered trademark of Chevron Intellectual Property, LLC, Houston, Texas.

Figure 3. Locations of monitoring sites and surface meteorological stations for the Boston Logan International Airport 2024 study.

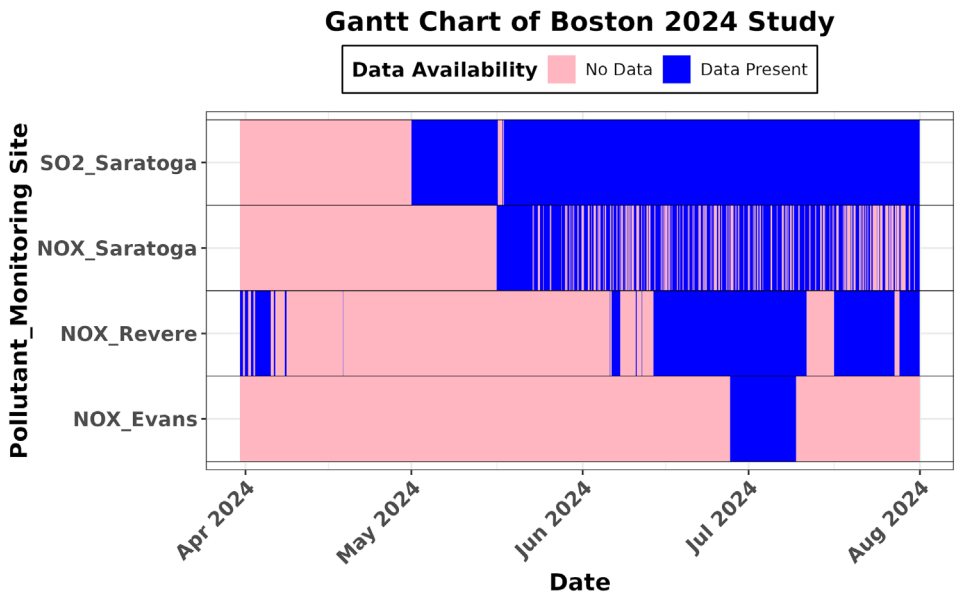

Figure 4. Data availability at all four sites for sulfur dioxide (SO_2) and nitrogen oxides (NO_x) pollutants in the Boston Logan International Airport 2024 study.

Table 2. Data availability at all four sites for sulfur dioxide (SO_2) and nitrogen oxide (NO_x) pollutants in the Boston Logan International Airport 2024 study.

Pollutant	Site	Data Available Day (Hours)	Total Day (Hours)	Data Availability (%)
SO_2	Saratoga	91 (2186)	123 (2952)	74.05
NO_x	Saratoga	53 (1266)	123 (2952)	42.89
	Revere	49 (1186)	123 (2952)	40.18
	Evans	12 (287)	123 (2952)	9.72

2.1.2.2.2 Meteorological Data Input

To create the meteorological input files to run AERMOD for the 2024 spring/summer season, it was necessary to run AERMET, the meteorological preprocessor for AERMOD. For this, hourly surface meteorological data were acquired from the weather station at BOS (WMO 72509 or WBAN 14739) (Figure 3) for the spring/summer of 2024, including 1-min and 5-min wind data. The nearest radiosonde station in Gray, Maine (KGYX) (WMO 74389 and WBAN 54762), was used for upper air data. AERMINUTE (version 15272) uses 1-min and 5-min data to generate a more accurate average wind condition for each hour than the data from the surface weather station. AERMET (version 24142) was run with the ADJ_U* option enabled. The AERSURFACE tool (version 20060) was used to estimate surface roughness length, albedo, and Bowen ratio for the study. Land cover, impervious, and canopy data files from 2016 were used as inputs for the tool to generate the necessary input files for AERMET. Twelve equally distributed sectors were drawn around the airport's weather station with a radius of 1 km. All land-use sectors were assigned as Airport.

Figure 5 represents the wind rose plot for the 2024 spring/summer season, showing the frequency of counts by wind direction as a percentage. During the study period, most of the winds are westerly or southwesterly (Figure 5). This wind rose plot suggests that the Saratoga and Revere sites were downwind during the study, and the Saratoga site was impacted by aircraft emissions through south-westerly winds.

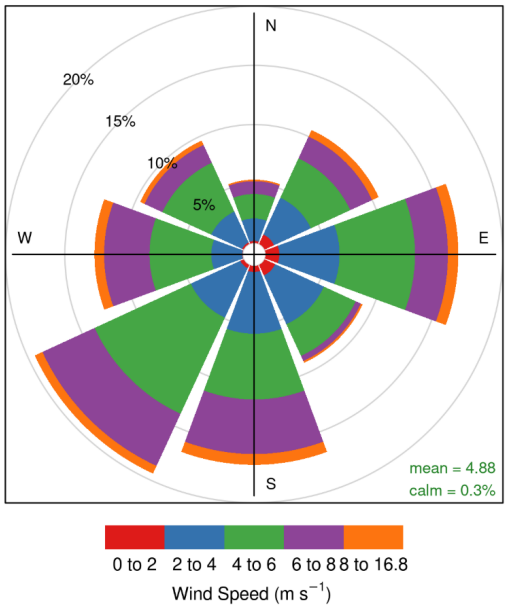

Figure 5. Wind rose plot of the 2024 spring/summer season, showing the frequency of counts by wind direction as a percentage for the Boston Logan International Airport 2024 study.

2.1.2.2.3 Observation Data

The observed SO_2 and NO_x concentration distributions are presented in box-and-whisker plots for each hour of the spring/summer season in Figure 6 and Figure 7 below, with one monitoring site and three monitoring sites, respectively. In Figure 6 and Figure 7, the boxes' top, middle, and bottom edges indicate 75th, 50th, and 25th percentile values, and the top and bottom whiskers show the values corresponding to 1.5 times the interquartile range (IQR). The colors of the dots on each plot represent the wind direction, whereas hollow black dots represent the mean value of overall concentrations for each hour. The higher SO_2 concentrations were measured at the Saratoga site from 7 AM onwards due to the southwesterly wind (180–270 degrees wind sector) contributions (Figure 6). There was a constant 0.1 ppb value at each hour that represents the minimum detection level (LOD) value (Figure 6).

The NO_x concentrations also have the same patterns as SO_2 at each hour for the Revere and Saratoga sites (Figure 7). The higher NO_x concentrations occurred in the early morning and late-night hours when the winds were south-westerly, which suggested that there was a strong signal of aircraft-related activity at these sites. On the other hand, at Evans, when the winds were north easterly or north westerly, we see the higher concentrations and aircraft-related contributions.

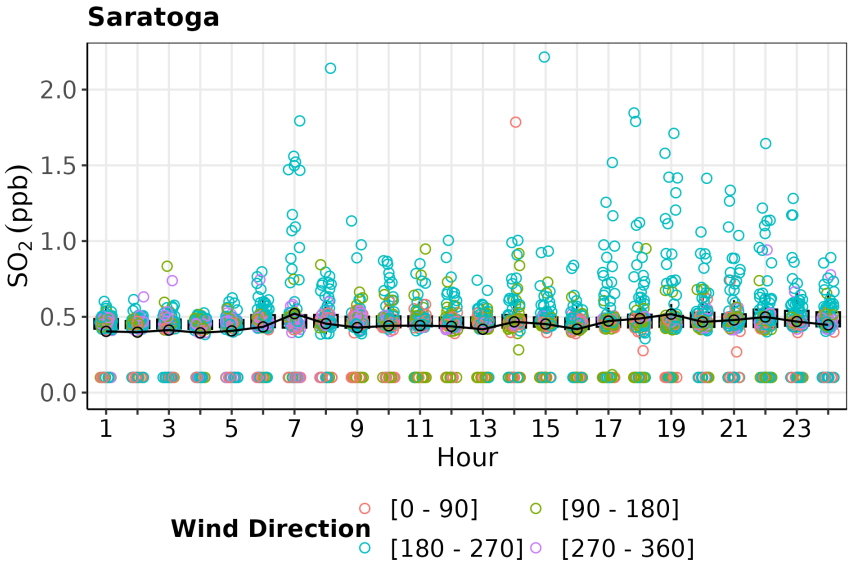

Figure 6. Box-and-whisker plots of measured sulfur dioxide (SO_2) concentrations at the Saratoga site during the 2024 spring/summer season for the Boston Logan International Airport 2024 study. Black hollow dots represent the mean value of overall concentrations at the site for each hour.

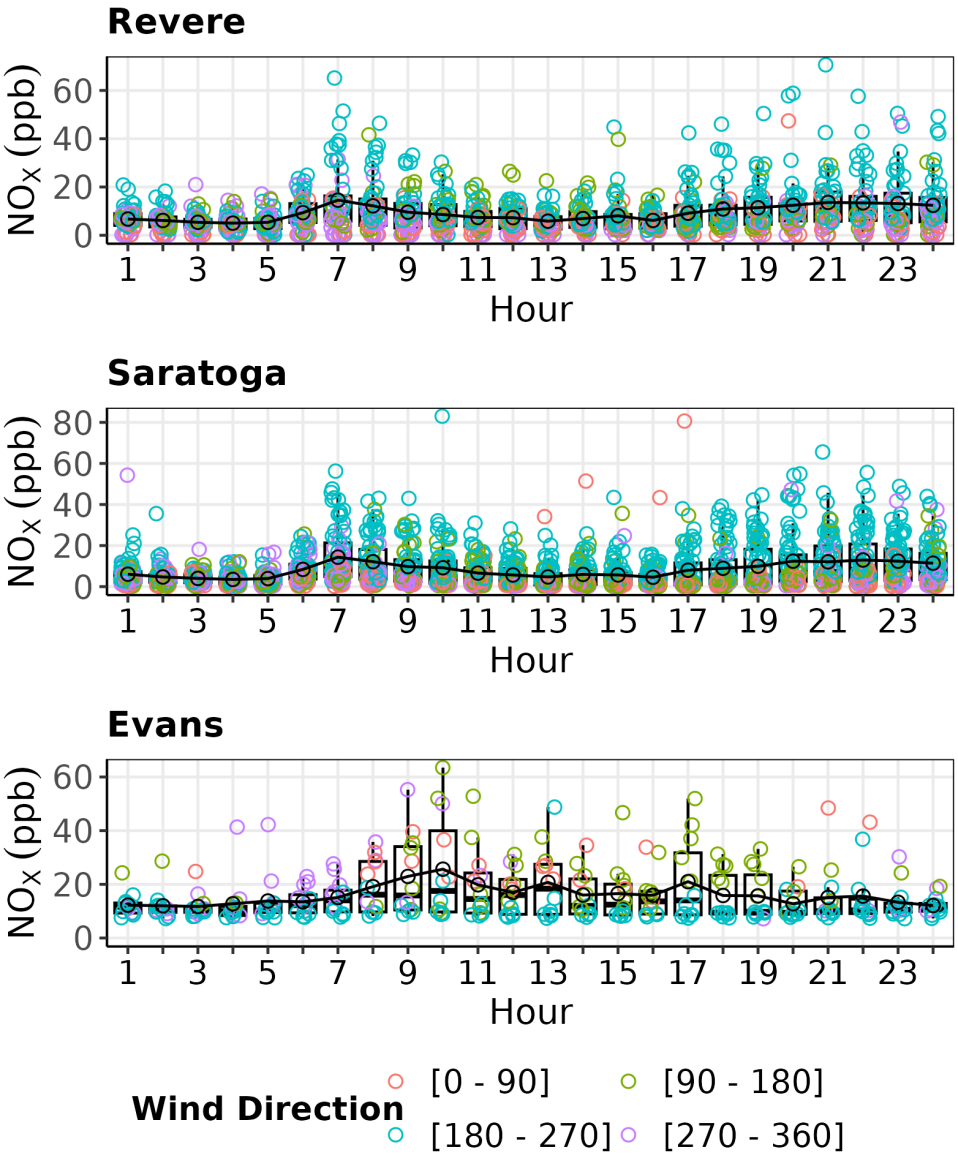

Figure 7. Box-and-whisker plots of measured nitrogen oxide (NO_x) concentrations at the Revere, Saratoga, and Evans sites during the 2024 spring/summer season for the Boston Logan International Airport 2024 study. Black hollow dots represent the mean value of overall concentrations at each site for each hour.

2.1.2.2.3.1 Additional Observation Data Analysis

To compare the pollutant concentration values at BU monitoring sites (Revere, Saratoga, and Evans) with nearby monitoring sites, we collected Air Quality System (AQS) data at other sites located within a 50-km radius of BOS for the 2024 study period. BU had provided UNC-IE with the cleaned hourly observation datasets for nitric oxide (NO), NO_2, and total NO_x at Evans, Revere, and Saratoga, MA, as well as cleaned SO_2 data at Saratoga. The locations of these sites are labeled in Figure 8, and data sources are denoted with "(BU)" for Boston University monitoring sites and "(EPA)" for background AQS monitoring sites.

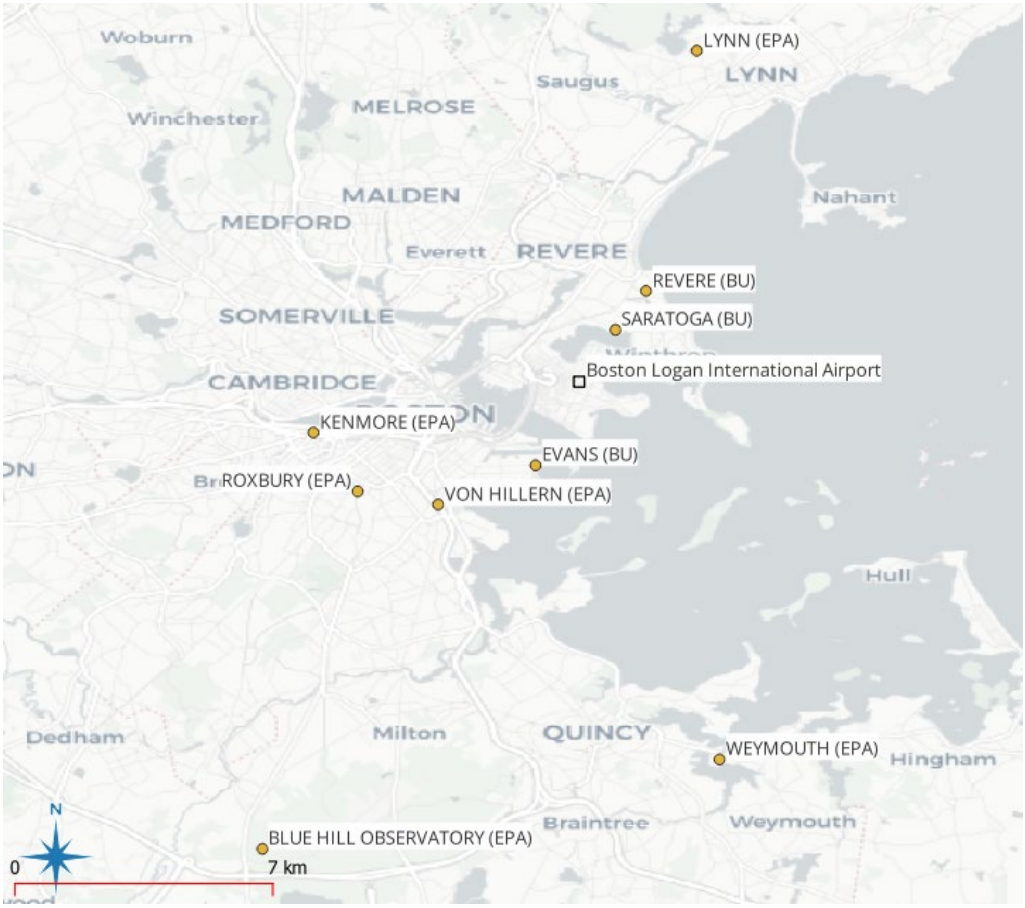

Figure 8. Boston Logan International Airport monitoring sites within 50km, denoted with "(BU)," and EPA AQS background monitoring sites, denoted with "(EPA)," over the Boston region.

We conducted a comparative analysis between the BU monitoring data and the background AQS monitoring site data (Figure 9). Based on the temporal coverage and data completeness, the study period of March 31 to July 31, 2024, was selected. We found that both types of monitoring sites had reasonable concentration values, and sites with relatively lower and higher concentrations were explained based on their farther or closer proximity to center-city Boston, respectively.

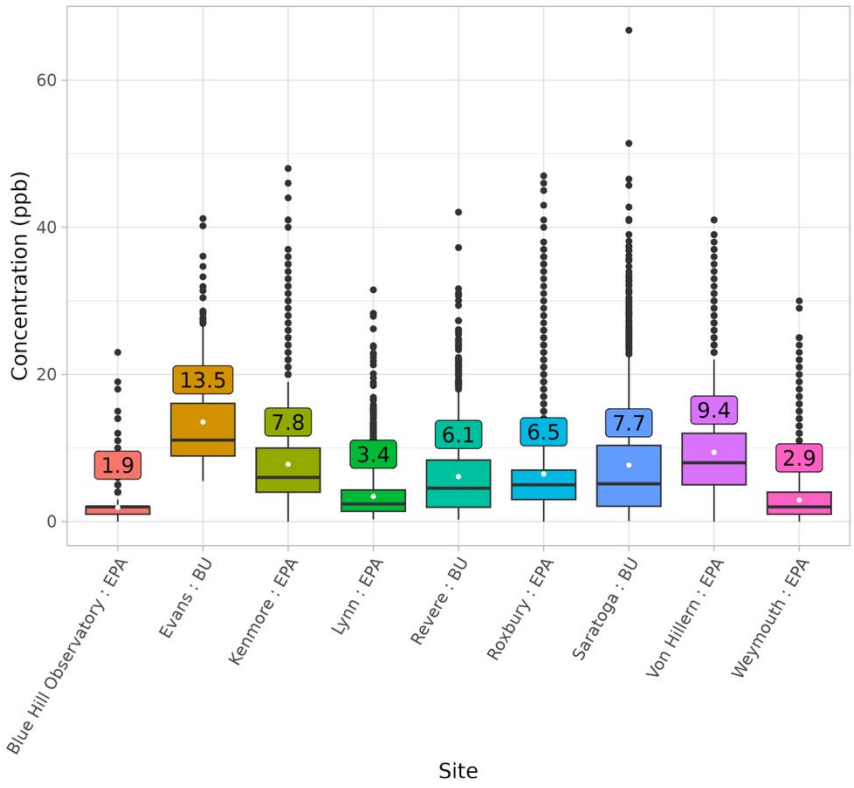

Figure 9. Box and whisker plots of NO_2 hourly concentrations at BU monitoring sites and AQS background sites from 3/31/2024 to 7/31/2024 (Values in each box and whisker indicate the means of the distributions). BU: Boston University, EPA: U.S. Environmental Protection Agency.

2.1.2.2.4 Emissions Data

Aircraft emissions of SO_2 and NO_x were calculated using the FAA's AEDT, which models all the LTO models as distinct area sources of varying sizes. This emissions dataset was provided by the U.S. Department of Transportation Volpe Center (Volpe). Non-aircraft emissions were extracted from EPA's Emission Modeling Platform version 2022v1. Here, we describe the processing of aircraft and non-aircraft emissions for this study.

2.1.2.2.4.1 Aircraft Emissions

AEDT is a publicly available software program used to support the research and regulatory compliance of aircraft and related airport-activity emissions. Using what is known as "threaded-track (TT) data" from the MITRE Corporation (MITRE), aircraft activity parameters are inserted into the AEDT model to estimate emissions at different segments of flights. Parameters such as aircraft engine and airframe specifications, operation type (i.e., arrival, departure, etc.), and operation times are combined with information in the AEDT program's integrated airport and aircraft database. With all these parameters, the AEDT can calculate fuel consumption, emissions, and generate AERMOD inputs for dispersion modeling.

Individual flight operations at BOS were acquired from MITRE for April–July 2024 and injected into the AEDT (version 3g) database using a series of scripts to process raw aircraft movements into the modeling domain and assign fleet data (i.e., unique airframe, engine type, and engine modification) to each operation. Aircraft operations were categorized as either arrivals or departures and assigned to one of the default flight profiles (which assigns the weight of the aircraft) within the AEDT based on the operation's stage length (related to the flight distance) and airframe. Operations were linked to specific runway ends based on the identifier provided in the raw dataset.

Information on aircraft ground movements was unavailable in the MITRE dataset. To estimate emissions from aircraft's taxi movements, operations were assigned to one of four terminal areas at the airport based on the airline operator named in

the flight operation. BOS has four terminals that aircraft use for commercial operations: A, B, C, and E. In general, terminals A, B, and C handle domestic air travel, while terminal E handles international air travel. BOS maintains a list of the terminals used by the different airline operators, by arrival and departure operations (source). The taxi network, which is made up of taxi paths and their associated taxiways, was manually created using satellite imagery of BOS. Taxiways in the AEDT are defined as a set of geographical points along which the aircraft travels, and taxi paths are a series of taxiways that link a runway end to a gate (or, in this case, terminal) and vice versa. Runway ends and terminals were linked via the shortest taxi route possible. AEDT's Delay and Sequencing Module (DSQM) then modeled aircraft ground movements given the defined taxi network and operations schedule. The DSQM ensures aircraft do not occupy the same location at the same time by creating queues as needed, thus determining the time an aircraft spends in taxi. Queues typically occur near the runway ends as aircraft are appropriately spaced for departures. The AEDT assumes arrival aircraft do not queue and taxi directly to their assigned terminal without delay.

For the AEDT to create the hourly emission (HRE) input files to run dispersion via AERMOD, it is necessary to run AERMET, the meteorological preprocessor to AERMOD. Files output from AERMET are used by the AEDT to model aircraft performance and thus calculate the associated emissions. For this evaluation, hourly surface meteorological data and upper air data files were taken, similar to those discussed in Section 2.1.2.2.2.

All emissions are aggregated to each modeling hour, by source, and are converted into AERMOD source-specific emission rates that can vary by hour (via HRE file). Calculated emissions from each flight operation were split across various ground and airborne segments. Within the dispersion workflow of the AEDT, emissions are only calculated for flights up to 914 m above field elevation (AFE). For this study, aircraft were from 914 m AFE up to 15 km from the airport on departure and up to 25 km from the airport upon arrival. The AEDT allocates airport-related emissions into spatially fixed emission sources that can be read by AERMOD. Aircraft sources were defined using default AEDT preferences; the study was run twice – once with aircraft emissions characterized by area sources with plume rise implementation and once without plume rise implementation. When using AREA source characterization, aircraft on the ground were defined with areas of 20 m by 20 m, an initial vertical dispersion dimension of 4.1 m, and a release height of 12 m. Airborne emissions were characterized with 200 m by 200 m areas spaced every 20 m vertically starting at 22 m AFE until 300 m AFE. Emissions between 300 m AFE and 914 m AFE were represented by sources positioned halfway between, or 607 m AFE. Additionally, the initial lateral dispersion dimension was based on an initial lateral dispersion dimension ratio of 4.3 per the EPA-suggested value in the AERMOD User's Guide. Additional details on how AEDT 3g sets up the AERMOD input files can be found in the AEDT 3g Technical Manual (Ross et al., 2024).

2.1.2.2.4.1.1 Reproduction of Aircraft Spring/Summer Emissions

We received the .bak file for the 2024 AEDT BOS study from Volpe in December 2024. In March 2025, UNC-IE received methodological documentation from Volpe describing the setup of the 2024 BOS Study within the AEDT. The study was built using aircraft-movement data from MITRE to provide necessary inputs to the AEDT model. In the methodological documentation, Volpe detailed the steps taken to process the MITRE data into a format usable for AEDT. UNC-IE developed its own series of Structured Query Language (SQL) scripts based on this documentation to process the MITRE data according to the criteria needed for a dispersion study in the AEDT. This also involved matching aircraft information in the MITRE data to the pre-existing set of aircraft data available in the AEDT FLEET database. Since UNC-IE was attempting to recreate the study using their own scripting approach, and the exact nuances in Volpe's approach were not defined, the process of aligning the aircraft the same as the original study became difficult to replicate. After some months on this task, UNC-IE and Volpe agreed that pre-processed MITRE data with AEDT-assigned aircraft information would be provided to support the process of replicating the study. Since aircraft information is linked to AEDT data using the best available information, there is not always a one-to-one match for an aircraft profile. This introduces some randomization and best-guess approaches, which make the aircraft assignments nearly impossible to entirely replicate. Even when Volpe provided the pre-processed MITRE data with FLEET assignments, it did not entirely match their original study setup. The taxi network configurations remained the same as the settings defined by Volpe in the original setup. Tracks were created for each air operation based on runway information provided in the MITRE dataset and airport layout information already included in the AEDT for BOS.

We collaborated with Volpe over several months to replicate the original study as accurately as possible, holding several calls to troubleshoot any issues that had arisen in the process. By the end of June 2025, UNC-IE successfully reproduced the study configuration. However, the results from both the Volpe and UNC-IE simulations were later determined to be preliminary, as subsequent review identified an issue in the taxi configuration setup that inadvertently increased taxi

segment lengths. UNC-IE will resolve these issues and will perform the AERMOD evaluation again using the updated AEDT aircraft emissions during the next period of performance.

2.1.2.2.4.2 Non-Aircraft Emissions

UNC-IE developed a comprehensive non-aircraft emissions inventory for BOS using a 1.33 km by 1.33 km gridded domain covering an 18.2 km by 16.9 km area over BOS (Figure 3, Figure 10). Non-aircraft emissions were filtered out from EPA's Emission Modeling Platform version 2022v1 (EMP2022v1)[5] for relevant sources within the domain and subsequently processed by using the SMOKE model version 5.1.[6] Non-aircraft emissions consider both surface and elevated source types. Surface source types include residential wood combustion (rwc), livestock, open burnings, mobile vehicles (on-road), solvents usages, non-road vehicles and equipment (non-road), railway and terminals, and others. Elevated source types include oil and gas production and processing, energy generation facilities, commercial marine vessels (CMV), and other industrial and commercial point sources. Emissions from surface source types were mapped to the 1.33 km by 1.33 km grid cells, each simulated as area sources in AERMOD. Elevated source types were processed at a facility-specific level and were simulated in AERMOD as point sources with associated coordinates and stack parameters. Temporal profiles provided with the EMP2022v1 were applied to non-aircraft emissions to aggregate annual emissions from short tons per year to hourly emissions in grams per second as required by AERMOD.

Special treatments to CMV emissions improved the accuracy of its spatial distributions. We derived these from geographic information system (GIS) datasets points of actual CMV activities, including shipping channels and seaport locations (Figure 10). Emissions were allocated based on quadrant location and channel depth, with activity fractions calculated for both port and underway points. Nonpoint sources, such as residential wood combustion, nonroad, and rail, were processed using SMOKE at an hourly resolution per grid cell. A tool was developed to convert these outputs into AERMOD-ready files, simulating each grid cell as a squared AREA source. Source grouping strategies were evaluated based on emission strength and proximity to monitoring sites. The approach was revised to use National Emission Inventory (NEI) 2022v1 directly, improving spatial and temporal accuracy over the original plan to scale NEI 2017 data, and daily AERMOD-ready outputs were generated for April through August 2022.

[5] https://www.epa.gov/air-emissions-modeling/2022v1-emissions-modeling-platform
[6] https://www.cmascenter.org/smoke/

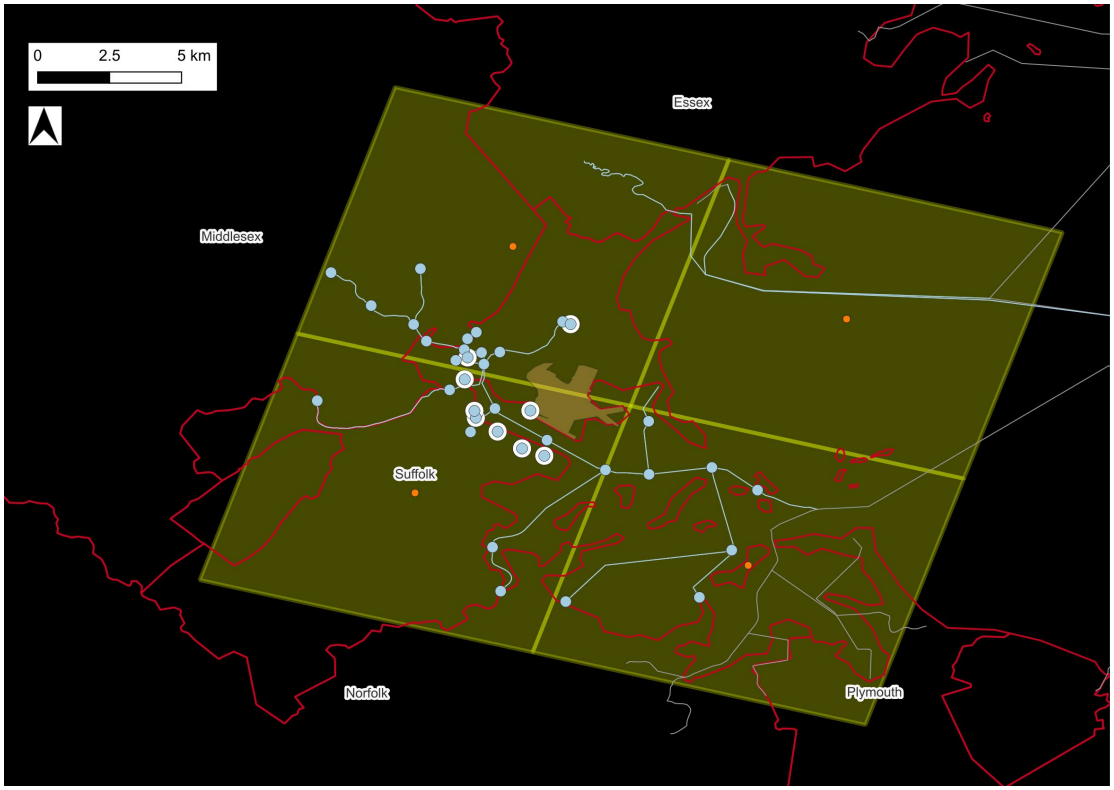

Figure 10. The GIS representation shows the relevant 12 km grid cells (yellow) overlaid on top of our domain with county boundaries in red and the airport footprint in brown. Also shown are the selected lines from the National Waterway Network Lines (NWNL), representing shipping channels (grey) that intersected our domain (light blue), and NWNL start and end points to represent underway activity (blue points). Seaport locations from Massachusetts Department of Environmental Protection's online GIS portal (white/blue dots) were used as port locations for hoteling emissions. Several underway points located in grid 191-388 were removed to simplify processing due to low emissions in that corresponding grid cell, as the vast majority of underway emissions were allocated to grid cells 190-387, 190-388, and 191-387.

Overall, the contribution of aircraft emissions was substantial when compared to non-aircraft sources, representing about 82% of the SO_2 and 26% of the NO_x emissions, respectively (Table 3). This highlights that aircraft were a dominant source of SO_2 emissions and a significant contributor to NO_x emissions within the BOS study area.

Table 3. Total tons per day of sulfur dioxide (SO_2) and nitrogen oxides (NO_x) aircraft and non-aircraft emissions in the 2025 spring/summer season for the Boston Logan International Airport study.

Source Type	Pollutant/Emissions (tons per day)	
	SO_2	NO_x
Aircraft	0.41	4.96
Non-Aircraft	0.50	19.24

2.1.3 Model Results

AERMOD modeled concentrations were compared with the observed SO_2 and NO_x concentrations from the LAX and BOS studies. To better understand how aircraft emissions affect air quality at the core monitoring sites, we analyzed concentrations based on prevailing wind sectors. We grouped the concentrations into 18, 20-degree wind direction sectors: (0 – 20], (20 – 40], (40 – 60], (60 – 80], (80 – 100], (100 – 120], (120 – 140], (140 – 160], (160 – 180], (180 – 200], (200 –

220], (220 – 240], (240 – 260], (260 – 280], (280 – 300], (300 – 320], (320 – 340], and (340 – 360], to assess how emissions from different directions influence each receptor site.

To evaluate the impact of our AERMOD model modifications, we compared results at the four core sites for the summer season of the LAX study and at three sites in spring/summer for the BOS study. This analysis was included: (i) ratio of mean modeled and mean measured concentrations at each site for various wind sectors, and (ii) hourly quantile-quantile (Q-Q) distribution plots at each site for filtered wind directions based on the prevailing wind sectors to assess the impact of aircraft emissions. In addition to this, this study also included model performance using common statistical measures, such as fractional bias based on the top 26 robust highest concentrations (FB) (Cox and Tikvart, 1990) and fraction of model predictions within a factor of two of the corresponding measurements (FAC2) (Chang and Hanna, 2004). These statistical measures are recommended by EPA to measure the performance of any dispersion model, especially for regulatory applications. Overall, these measures helped to determine how accurately the modified AERMOD reproduces observed concentrations.

The different model scenarios in AERMOD, with and without aircraft plume rise options, and with and without shoreline meteorology, were named as:

a. *Default*: The meteorological inputs were baseline AERMET outputs, and the plume rise option within AERMOD (version 24142) is not modeled. This corresponds to the default AERMOD setting that was normally used to predict the air quality impact of aircraft-related emissions.
b. *Old Plume Rise*: Same as 1., except that plume rise was modeled using the ALPHA option "ARCFTOPT" of AERMOD (version 24142); the methodology was described in Pandey et al. (2023).
c. *New Plume Rise*: Same as 1., except that the aircraft plume rise option used the updated plume rise algorithm described in this paper in Section 2.
d. *Shoreline OldPR*: Same as 2. except that the meteorological inputs were modified to account for shoreline and urban effects described in Pandey et al. (2022). This scenario was applicable only for the LAX study.
e. *Shoreline NewPR*: Same as 3., except that the meteorological inputs were modified to account for shoreline and urban effects described in Pandey et al. (2022). This scenario was applicable only for the LAX study.

2.1.3.1 Los Angeles International Airport Study

2.1.3.1.1 Concentrations Averaged over Wind Direction Sectors

Figure 11 and Figure 12 compared the model-predicted mean SO_2 and NO_x concentrations (from the five model scenarios described in Section 2.1.3 above), averaged over 18 wind direction sectors of 20 degrees, with the corresponding observed/measured mean concentrations at the four core sites (AQ, CN, CS, and CE) for the summer season in the LAX study. The dashed line (-----) represents the one-to-one line. The solid lines above and below the one-to-one line on the y-axis correspond to a factor of two intervals.

Here, we see differences across all five model scenarios. However, to understand which specific wind sectors affect each monitoring site, first, we need to focus on the comparison between the *Default*, *Old Plume Rise*, and *New Plume Rise* scenarios. By examining how these three differ, we can identify the specific wind direction sectors that contribute most to the ratio of modeled to measured concentration variations at each site. In contrast, for wind sectors where all three scenarios produce overlapping concentration patterns, we infer that the plume rise treatment had little to no impact, and the results are largely consistent across these three model scenarios.

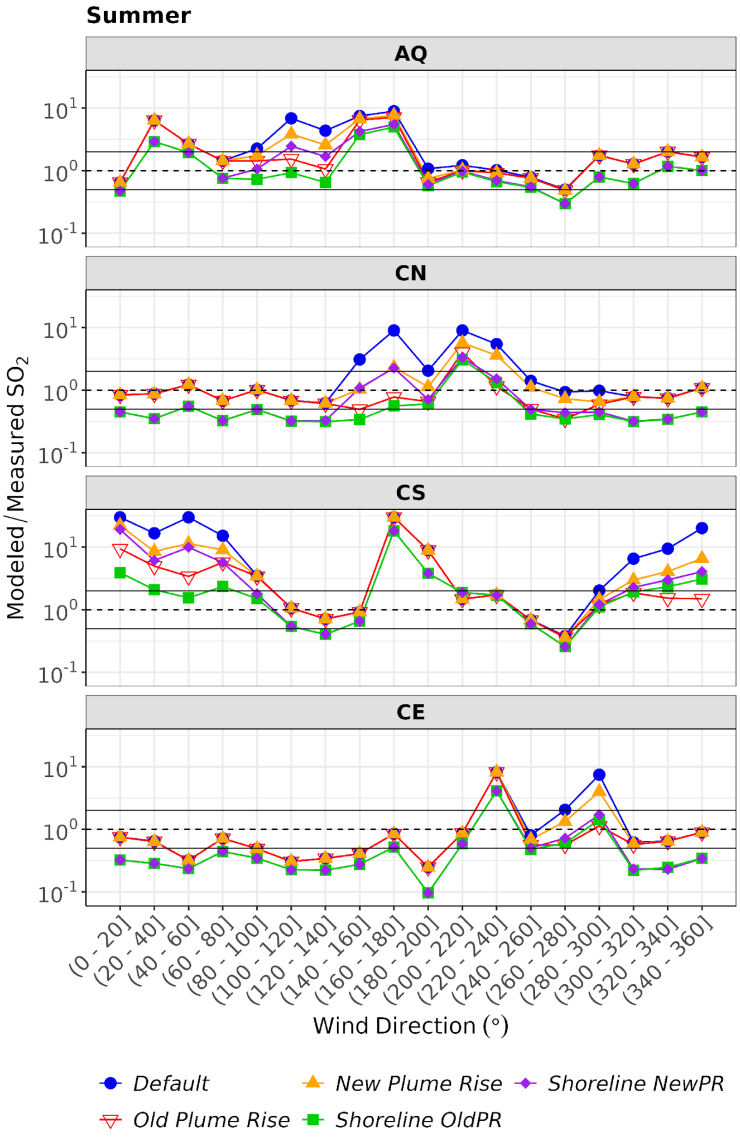

Figure 11. Ratio of modeled to measured SO_2 concentrations at all four core sites (AQ, CN, CS, and CE) during the 2012 summer season at Los Angeles International Airport.

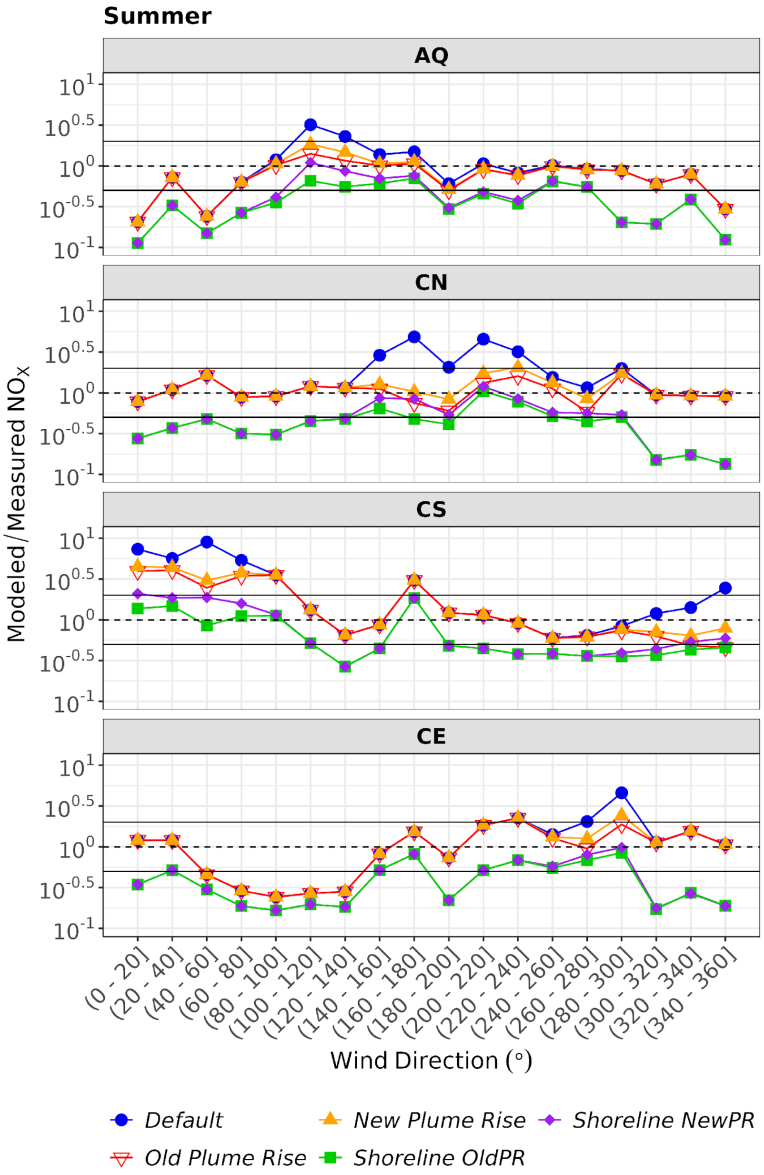

Figure 12. Ratio of modeled to measured NO_x concentrations at all four core sites (AQ, CN, CS, and CE) during the 2012 summer season at Los Angeles International Airport.

2.1.3.1.1.1 Sulfur Dioxide Concentrations

In Figure 11, there are noticeable differences across the *Default*, *Old Plume Rise*, and *New Plume Rise* model scenarios on the wind sectors at: AQ site (80 – 100], (100 – 120], (120 – 140], (140 – 160], (160 – 180], and (180 – 200]; CN site (140 – 160], (160 – 180], (180 – 200], (200 – 220], and (220 – 240]; CS site (0 – 20], (20 – 40], (40 – 60], (60 – 80], (280 – 300], (300 – 320], (320 – 340], (340 – 360]; and CE site (240 – 260], (260 – 280], (280 – 300] in both seasons. Other than these sectors, the differences across these three model scenarios were little to almost negligible at each site for both seasons.

From this, we can evaluate the performance of all five model scenarios at these site-specific wind sectors. Here, we hypothesize that *Shoreline NewPR* should perform better than other scenarios, as it had both new modifications: one based on the updated aircraft plume rise algorithm and the second, as Pandey et al. (2022) discussed, based on meteorology.

In Figure 11, *Shoreline NewPR* predicted the modeled to measured SO_2 values mostly on the one-to-one line, and only a few instances were within a factor of two lines across all the impacted wind sectors at all sites except site CS, where it was reducing the peaked values but not within the FAC2 lines, as the *Default* model predictions were higher compared to the other sites. Overall, the updated aircraft plume rise algorithm is enhancing the concentrations compared to the old plume rise algorithm, as the updated plume rise algorithm predicted the low plume rise values better.

2.1.3.1.1.2 Nitrogen Oxides Concentrations

NO_x concentration results were similar to SO_2 at all four core sites. NO_x ratio results exhibited patterns similar to those observed for SO_2, with *Shoreline NewPR* predictions aligning closely with the one-to-one line, and most values falling within the FAC2 range across the impacted wind sectors at all sites, except for CS, where peak values were reduced but still fall outside the FAC2 range due to the *Default* scenario's higher predictions, especially on (0 – 20], (20 – 40], (40 – 60], (60 – 80] wind sectors (Figure 12).

Based on all the prevailing wind direction findings, in the next section, we have presented hourly quantile-quantile distribution plots at each site for filtered wind sectors to assess the impact of aircraft emissions.

2.1.3.1.2 Overall Concentration Distribution Analysis (Quantile-Quantile Distribution Analysis)

For strong model performance and capability, especially for air quality regulation, it is important to predict high concentrations accurately. To assess this, unpaired concentration distribution plots, commonly referred to as Q-Q plots, were utilized. In these plots, both modeled and observed concentrations were first filtered based on the airport-impacted wind direction, as discussed in Section 2.1.3. At the CN site, we increased the wind direction bin from [140 – 240] to [140 – 250] to include the partial plume rise effect on the next wind direction bin concentrations. Similarly, at the CS site, we filtered the concentrations from 270 degrees instead of 280 degrees, because in the (260 – 280] bin, we could see a slight change from the *Default* to *New Plume Rise* scenario. After that, we ranked from highest to lowest and then plotted against each other. The dashed line (------) represents the one-to-one relationship, indicating a perfect agreement between modeled and observed values. The solid lines with slopes of one-half and two denote underpredictions and overpredictions, respectively. The Q-Q plots were developed using 1-hr averaged SO_2 and NO_x concentrations for both winter and summer seasons, comparing our five model scenarios: *Default*, *Old Plume Rise*, *New Plume Rise*, *Shoreline OldPR*, and *Shoreline NewPR* (see Figure 11 and Figure 12).

2.1.3.1.2.1 Sulfur Dioxide Concentrations

The high- to mid-range concentrations improved substantially from *Default* to *New Plume Rise* and even further with the *Shoreline NewPR* scenario at all sites (Figure 13). At AQ and CS sites, the overpredictions were improved with *Shoreline NewPR,* but there was still a slight overprediction, especially at higher concentrations (Figure 13). On the other hand, at the CN site, most of the concentrations fell a one-to-one line with the *Shoreline NewPR* scenario, and at the CE site, high concentrations came close to a one-to-one line (Figure 13).

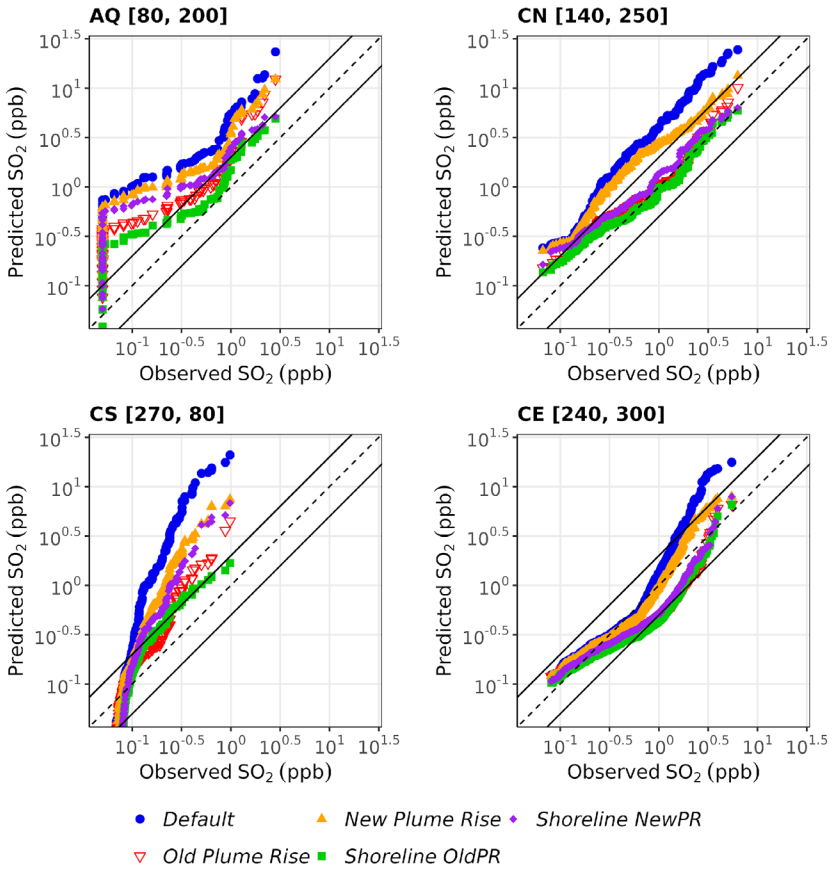

Figure 13. Q-Q plots show the effect of aircraft-specific plume rise and modifying meteorological inputs for the summer season SO_2 concentrations at each site for specific wind directions.

Since regulatory applications of AERMOD emphasize concentrations at the upper end of the modeled distribution, it was important to evaluate the modified model's performance using statistics derived from the top 26 robust highest modeled and observed concentrations, as recommended by EPA (Cox and Tikvart, 1990). These statistics are summarized in Table 4.

Table 4. Fractional Bias (FB) based on the top 26 highest SO_2 concentrations, FAC2 (factor of two), and the ratio of robust highest SO_2 concentrations (Ratio_RHC) for the 2012 summer season.

Site	Model	Statistical Measures		
		FAC2 (%)	FB	Ratio_RHC
AQ [80, 200]	*Default*	1	-1.51	7.17
	Old Plume Rise	25	-1.15	3.72
	New Plume Rise	1	-1.28	4.56
	Shoreline OldPR	51	-0.71	2.10
	Shoreline NewPR	12	-0.82	2.39
CN [140, 250]	*Default*	0	-1.32	4.85
	Old Plume Rise	98	-0.46	1.60
	New Plume Rise	6	-0.65	1.97
	Shoreline OldPR	99	0.16	1.17
	Shoreline NewPR	88	-0.20	1.22
CS [270, 80]	*Default*	36	-1.85	25.84
	Old Plume Rise	81	-1.21	4.09
	New Plume Rise	44	-1.60	9.04
	Shoreline OldPR	63	-0.59	1.84
	Shoreline NewPR	37	-1.49	6.82
CE [240, 300]	*Default*	89	-1.25	4.37
	Old Plume Rise	79	-0.21	1.23
	New Plume Rise	100	-0.69	2.06
	Shoreline OldPR	69	-0.01	1.01
	Shoreline NewPR	100	-0.13	1.14

The fractional bias (FB) was defined by:

$$FB = 2\frac{(Measured - Modeled)}{(Measured + Modeled)} \quad \text{(Eq. 4)}$$

FAC2 referred to the fraction of modeled values within a factor of two of the corresponding measured/observed values. The ratio of the robust highest concentrations (RHC; Ratio_RHC), was the ratio of the modeled RHC to that of the measured, where the RHC of each set was computed using the 26 highest values. The positive FB and the values of the Ratio_RHC relative to unity suggested the underestimation of the highest pollutant concentrations during field study.

Table 4 shows the statistical measures from all five model scenarios at all four core sites. At all sites, the peak ratio (PR) based on top 26 robust highest concentrations improved significantly. At the AQ site, it improved from 7.17 to 2.39 when we used the *Shoreline NewPR* model scenario. At the CN site, it decreased from 4.85 to 1.22. At the CS site, it became closer to its ideal value of one, decreasing from 25.84 to 6.82, and at CE site, from 4.37 to 1.14. The fraction of model predictions to the observations, FAC2, also improved and more closely reached the ideal value of 100, especially at CN and CE sites.

2.1.3.1.2.2 Nitrogen Oxides Concentrations

At all sites, the *Default* scenario overpredicted higher NO_x concentrations, whereas, after the inclusion of plume rise, these higher concentrations better matched the one-to-one line (Figure 14). In addition, with *Shoreline NewPR,* all the high

concentrations at all sites came close to a one-to-one line, especially at the CN site; mid to high range concentrations lay on a one-to-one line (Figure 14). Table 5 shows the statistical measures for all model scenarios. Ratio_RHC was also improved significantly from 6.81 to 0.94, and 98% of concentrations were within a FAC2. At the CE site, *Shoreline NewPR* slightly underestimated the mid-level concentrations, whereas at the AQ and CS sites, the higher concentrations were still overpredicted but within FAC2 lines (Figure 14). Overall, at AQ and CS sites, the Ratio_RHC improved significantly and came closer to its ideal value of 1. FAC2 was also 99% and 49%, respectively, at these two sites (Table 5).

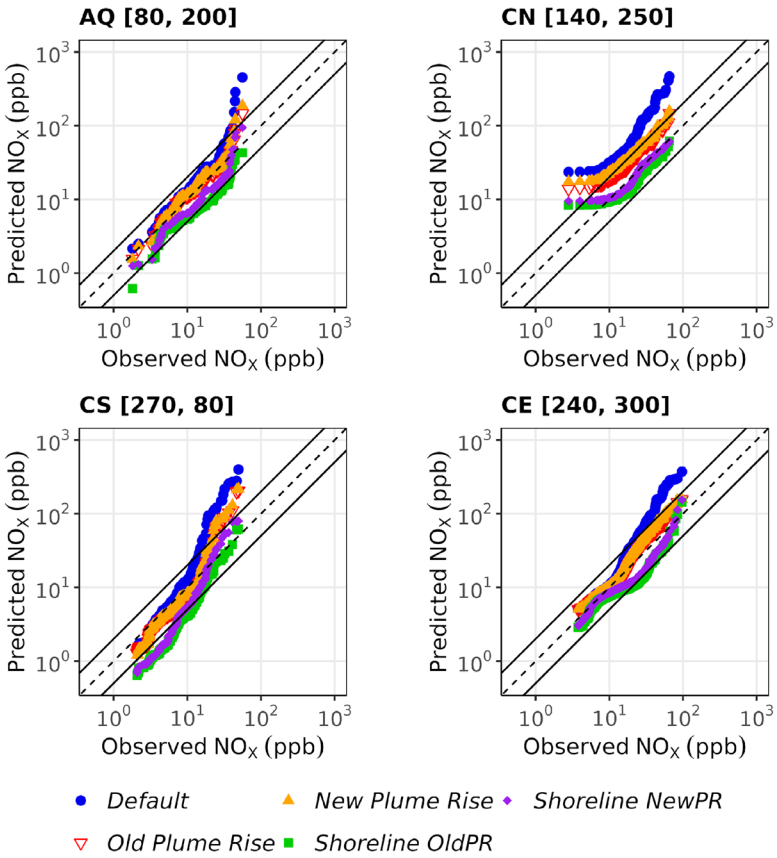

Figure 14. Q-Q plots show the effect of aircraft-specific plume rise and modifying meteorological inputs for the summer season nitrogen oxides (NO_x) concentrations at each site for specific wind directions.

Table 5. Fractional Bias (FB) based on the top 26 highest NO_x concentrations, FAC2 (factor of two), and the ratio of robust highest NO_x concentrations (Ratio_RHC) for the 2012 winter and summer seasons.

Site	Model	Statistical Measures		
		FAC2 (%)	FB	Ratio_RHC
AQ [80, 200]	*Default*	90	-1.27	4.45
	Old Plume Rise	98	-0.47	1.62
	New Plume Rise	97	-0.77	2.24
	Shoreline OldPR	65	0.29	0.74
	Shoreline NewPR	99	-0.22	1.25
CN [140, 250]	*Default*	0	-1.43	6.01
	Old Plume Rise	90	-0.59	1.84
	New Plume Rise	30	-0.70	2.07
	Shoreline OldPR	98	0.17	0.84
	Shoreline NewPR	98	0.06	0.94
CS [270, 80]	*Default*	82	-1.52	7.27
	Old Plume Rise	94	-1.13	3.57
	New Plume Rise	93	-1.18	3.89
	Shoreline OldPR	22	-0.07	1.07
	Shoreline NewPR	49	-0.59	1.84
CE [240, 300]	*Default*	82	-1.24	4.29
	Old Plume Rise	100	-0.38	1.47
	New Plume Rise	100	-0.51	1.69
	Shoreline OldPR	85	0.10	0.90
	Shoreline NewPR	100	-0.06	1.06

2.1.3.2 Boston Logan International Airport Study

2.1.3.2.1 Concentrations Averaged over Wind Direction Sectors

Figure 15 and Figure 16 compared the model-predicted mean SO_2 and NO_x concentrations (from three of the model scenarios described in Section 2.1.3: *Default*, *Old Plume Rise,* and *New Plume Rise*), averaged over 18 wind direction sectors of 20 degrees, with the corresponding observed/measured mean concentrations at Evans, Saratoga, and Revere sites (SO_2 at Saratoga only) for the spring/summer season in the BOS study. The dashed line (-----) represents the one-to-one line. The solid lines above and below the one-to-one line on the y-axis correspond to a factor of two intervals.

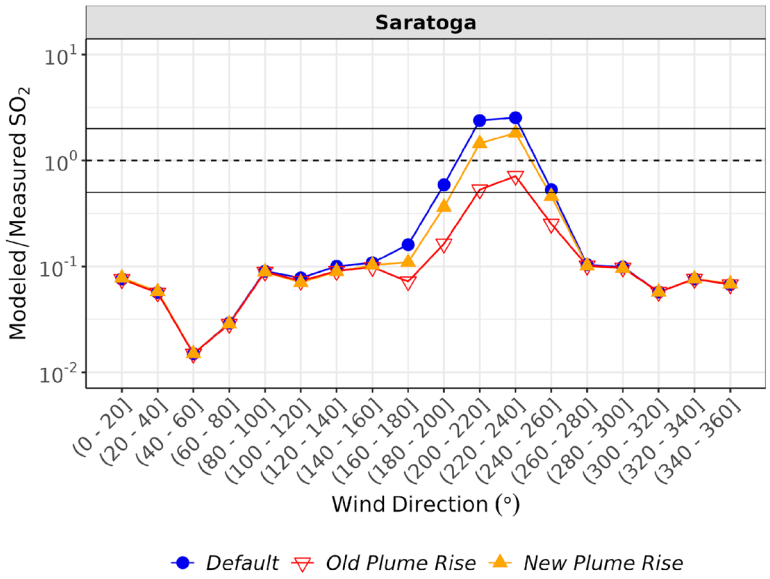

Figure 15. Ratio of modeled to measured sulfur dioxide (SO_2) concentrations at the Saratoga site, during the 2024 spring/summer season at Boston Logan International Airport.

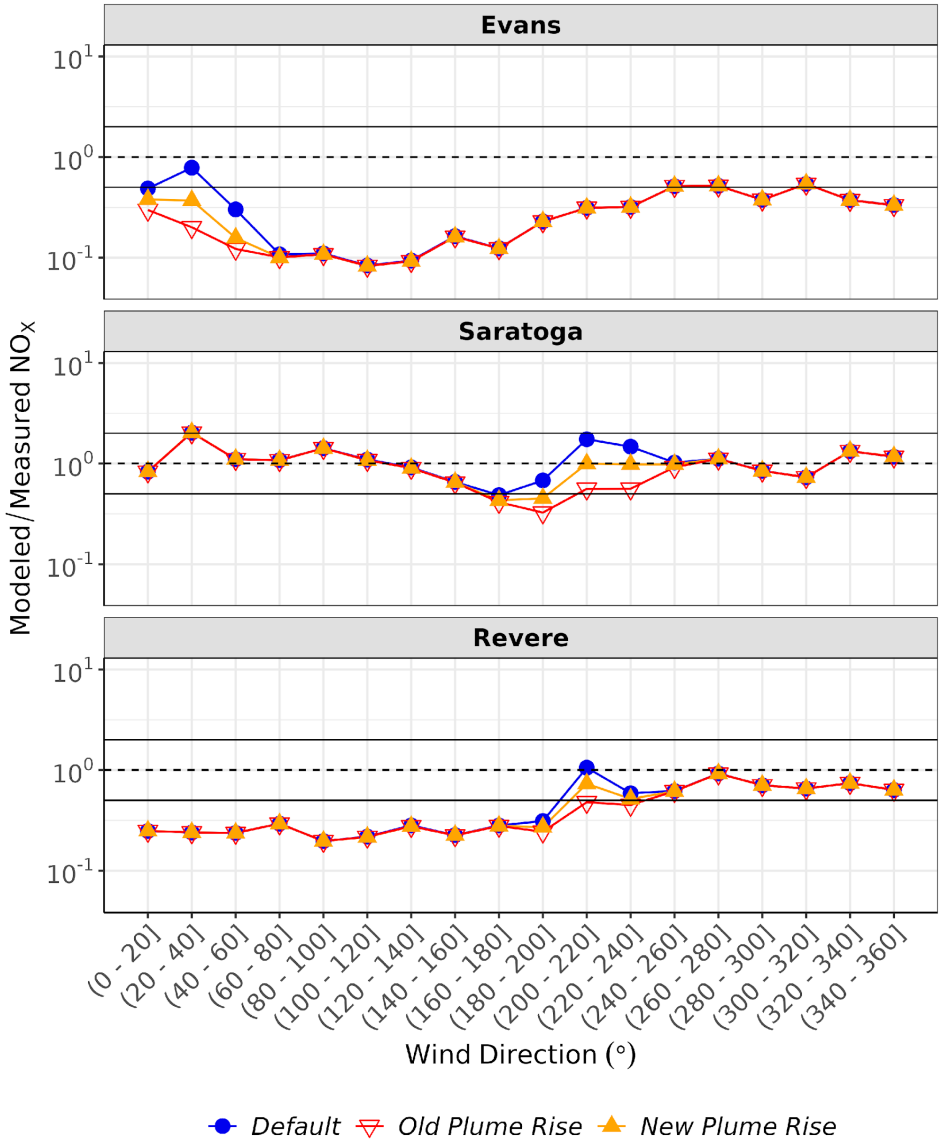

Figure 16. Ratio of modeled to measured nitrogen oxides (NO_x) concentrations at all three sites (Evans, Saratoga, and Revere) during the 2024 spring/summer season at Boston Logan International Airport.

Here, we see differences across all three model scenarios. However, to understand which specific wind sectors affect each monitoring site, first, we needed to focus on the comparison between the *Default*, *Old Plume Rise*, and *New Plume Rise* scenarios. By examining how these three differ, we can identify the specific wind direction sectors that contributed most to the ratio of modeled to measured concentration variations at each site. In contrast, for wind sectors where all three scenarios produced overlapping concentration patterns, we infer that the plume rise treatment had little to no impact, and the results are largely consistent across these three model scenarios.

2.1.3.2.1.1 Sulfur Dioxide Concentrations

In Figure 15, there are noticeable differences across the *Default*, *Old Plume Rise*, and *New Plume Rise* model scenarios on the wind sectors at: Saratoga site (160 – 180], (180 – 200], (200 – 220], and (220 – 240], and (240 – 260]. Other than these sectors, the differences across these three model scenarios were little to almost negligible.

In Figure 15, *New Plume Rise* predicted the modeled to measured SO_2 values slightly above the one-to-one line, and only a few were underpredicted and were not within a factor of two lines on all the impacted wind sectors, whereas with the *Old Plume Rise*, these values were highly underpredicted. Overall, the updated aircraft plume rise algorithm is enhancing the concentrations compared to the old plume rise algorithm, as the updated plume rise algorithm predicted the low plume rise values better.

2.1.3.2.1.2 Nitrogen Oxides Concentrations

For NO_x, the modeled-to-measured mean NO_x ratio results of the *New Plume Rise* model scenario were better compared to the *Old Plume Rise* model scenario, especially at the Saratoga site, where most of the values were on a one-to-one line in the wind direction bin from 200 to 260 degrees (Figure 16). At the Revere site, both *Old Plume Rise* and *New Plume Rise* model scenarios underpredicted the mean-modeled to mean-measured values for the impacted wind direction sectors 180 to 240 degrees, where we have seen a noticeable change from *Default* to any plume rise model scenario (Figure 16).

2.1.3.2.2 Overall Concentration Distribution Analysis (Quantile-Quantile Distribution Analysis)

The Q-Q plots were developed using 1-hour averaged SO_2 and NO_x concentrations for the 2024 spring/summer season, comparing three model scenarios: *Default*, *Old Plume Rise*, and *New Plume Rise*. Here, we filtered the observed/measured and modeled concentrations for specific wind sectors at each site (see Figure 15 and Figure 16).

2.1.3.2.2.1 Sulfur Dioxide Concentrations

At Saratoga, the mid to high SO_2 concentrations were highly overpredicted by the *Default* model scenario, whereas, after the inclusion of aircraft-specific plume rise *Old Plume Rise*, these high concentrations reduce substantially (highly underpredicted) (Figure 17). However, after updating the current plume rise algorithm, the model predications improved significantly and came close to a one-to-one line, but, still, there was a slight overprediction with the *New Plume Rise* model scenario (Figure 17).

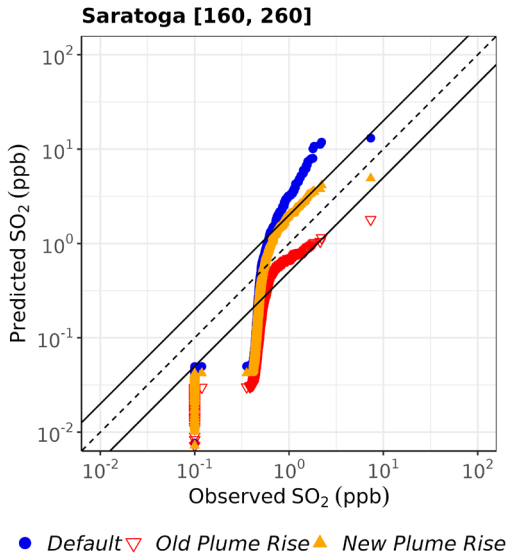

Figure 17. Q-Q plots showing the effect of aircraft-specific plume rise for the spring/summer season SO_2 concentrations at the Saratoga site for specific wind directions.

Table 6 summarizes the EPA-recommended statistics utilized. FAC2 was improved from 40 to 50% with the *New Plume Rise* model scenario. The significant improvement in the ratio of the top 26 robust highest concentrations came down from 4.30 to 1.50.

Table 6. Fractional Bias (FB) based on the top 26 highest SO_2 concentrations, FAC2 (factor of two), and the ratio of robust highest SO_2 concentrations (Ratio_RHC) for 2024 spring/summer seasons at Boston Logan International Airport.

Site	Model	Statistical Measures		
		FAC2 (%)	FB	Ratio_RHC
Saratoga [160, 260]	*Default*	40	-1.25	4.30
	Old Plume Rise	27	0.90	0.38
	New Plume Rise	50	-0.40	1.50

2.1.3.2.2.2 Nitrogen Oxides Concentrations

For NO_x concentrations, Figure 18 shows the Q-Q distributions at all three sites for the specific wind sectors at each site. At Evans, the *Default* model scenario overpredicted all concentrations, whereas with the inclusion of any plume rise, all of them fall within FAC2 lines and close to a one-to-one line. From Table 7, we observe that the ratio of the top 26 robust highest concentrations improved from 3.14 to 1.08, and FAC2 improved from 0 to 100% with the *New Plume Rise* model scenario.

At Saratoga and Revere, higher-end overpredictions from the *Default* model scenarios were significantly improved with the *New Plume Rise* scenario, and most of the mid to high range concentrations lay on a one-to-one line (Figure 18). Ratio_RHC improved from 3.96 to 0.91 and from 1.97 to 0.72 at Saratoga and Revere sites, respectively (Table 7).

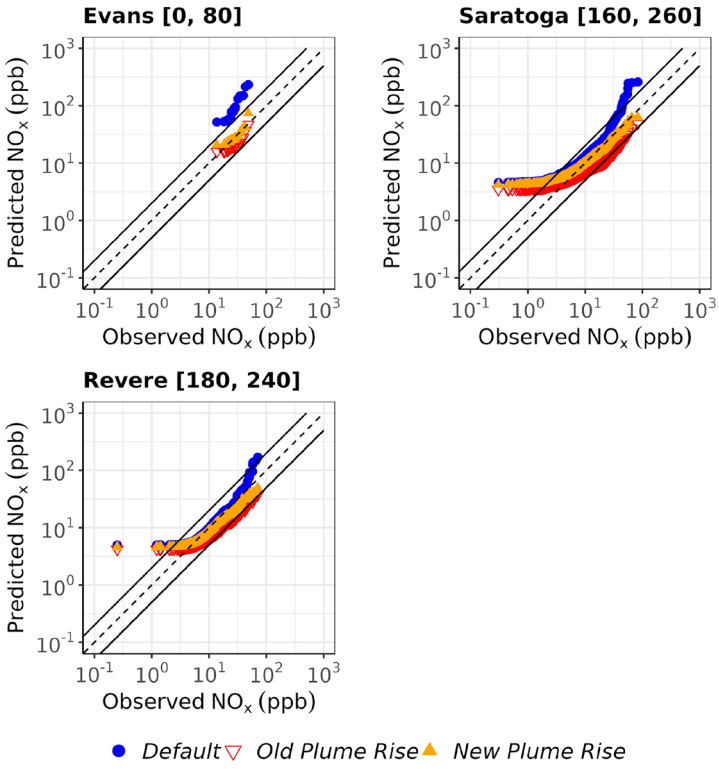

Figure 18. Q-Q plots showing the effect of aircraft-specific plume rise for the spring/summer season NO_x concentrations at each site for specific wind directions.

Table 7. Fractional Bias (FB) based on the top 26 highest NO_x concentrations, FAC2 (factor of two), and the ratio of robust highest NO_x concentrations (Ratio_RHC) for the 2024 spring/summer season.

Site	Model	Statistical Measures		
		FAC2 (%)	FB	Ratio_RHC
Evans [0, 80]	*Default*	0	-1.29	3.14
	Old Plume Rise	100	0.31	0.78
	New Plume Rise	100	-0.02	1.08
Saratoga [160, 260]	*Default*	85	-1.19	3.96
	Old Plume Rise	70	0.45	0.63
	New Plume Rise	92	0.09	0.91
Revere [180, 240]	*Default*	97	-0.65	1.97
	Old Plume Rise	91	0.62	0.63
	New Plume Rise	98	0.33	0.72

2.1.4 Summary

The effectiveness of incorporating the updated aircraft plume-rise option into AERMOD was evaluated by comparing modeled concentrations with field measurements, with a particular focus on wind directions most affected by aircraft emissions for the LAX 2012 and BOS 2024 field studies. For both SO_2 and NO_x, AERMOD's performance improved noticeably across all monitoring sites once the revised plume-rise formulation was applied. The *New Plume Rise* model scenario improved the modeled concentrations significantly, especially for mid to high range concentrations.

The updated algorithm generally produced lower plume-rise estimates for each aircraft LTO mode. These reduced plume-rise values led to higher near-field modeled concentrations, resulting in a better match with observed concentration values. The evaluation also demonstrated that the updated plume-rise approach performs consistently across different airports and study conditions, confirming the robustness and broad applicability of the new algorithm within AERMOD.

2.2 Los Angeles International Airport Summer Study Model Comparison against LASPORT

We received LASPORT (**LAS**AT (**La**grangian **S**imulation of **A**erosol **T**ransport) for Air**port**s) model SO_2 and NO_x results for the summer 2012 LAX AQSAS on September 15, 2025, from Dr. Ulf Janicke (Janicke Consulting, Germany).

LASPORT results only included aircraft, ground support equipment, and auxiliary power unit sources' contributions. For the comparison against AERMOD model results, we added the background source contributions (AERMOD modeled) with LASPORT results. We analyzed the modeled results using the original meteorology for the AERMOD model. For LASPORT, it had only one set of results, so it was assumed that these were generated using the original meteorology. Here, for model comparison, we used the following AERMOD model scenarios: *Default*: AERMOD without plume rise; *Old Plume Rise*: AERMOD with old plume rise (was implemented in AERMODv24142); *New Plume Rise*: AERMOD with new plume rise (updated recently as discussed above).

Figure 19 and Figure 20 show the Q-Q concentration distribution among models in original meteorology for SO_2 and NO_x pollutants, respectively.

Q-Q distribution plots for SO_2 show that LASPORT and AERMOD with the *New Plume Rise* model scenario are very close for mid to high range concentrations, especially at CN and CE (Figure 19). The PR (also referred to as the Ratio of RHC) based on the top 26 robust highest concentrations was slightly higher than its ideal value of one for both models, and the fraction of predictions within FAC2 values was better in *New Plume Rise* than LASPORT, especially at sites CN, CS, and CE (Figure 19).

In Figure 20, all model scenarios were overpredicting the higher concentrations at all sites.

Based on the above, we concluded that our *New Plume Rise* scenario performed as well as, if not better than, LASPORT under most conditions for both pollutants. However, one should note that LASPORT doesn't include a plume rise algorithm due to the potential to underestimate, instead focusing on parameterization of plume dynamics.

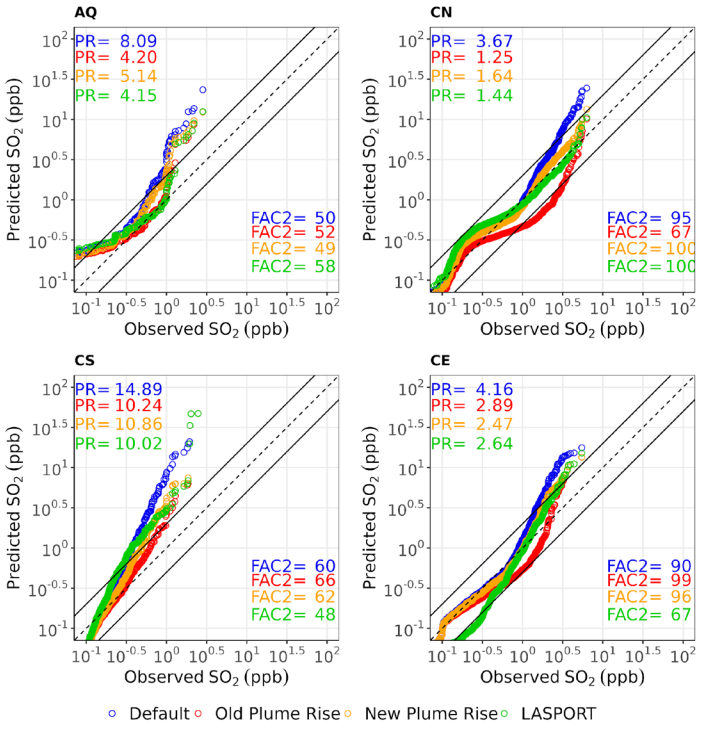

Figure 19. Q-Q distribution of SO_2 concentrations at all four core sites (AQ, CN, CS, and CE) for summer 2012 at Los Angeles International Airport. PR metric in these plots refer to peak ratio of robust highest concentrations. FAC2 refers to % predictions within a factor of two of observations.

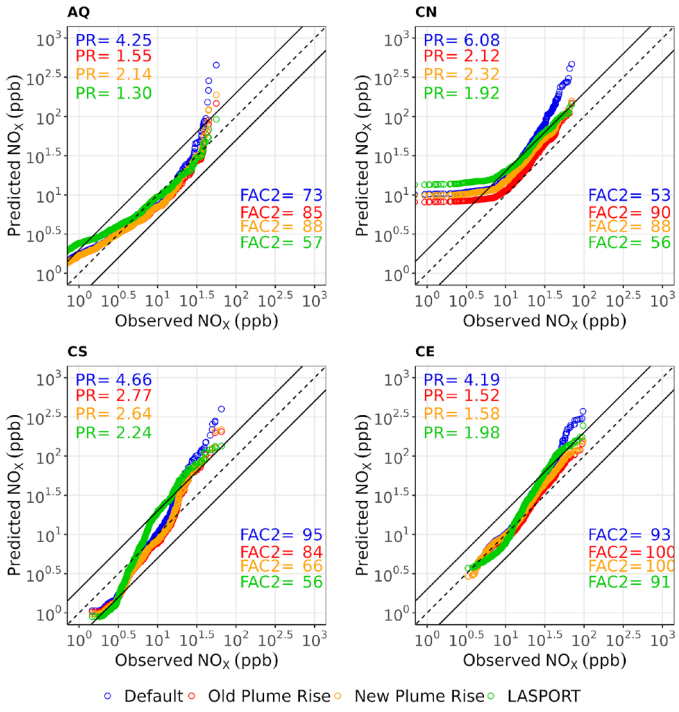

Figure 20. Q-Q distribution of NO_x concentrations at all four core sites (AQ, CN, CS, and CE) for summer 2012 at LAX. PR metric in these plots refer to peak ratio of robust highest concentrations. FAC2 refers to % predictions within a factor of two of observations.

3. Chemical Processes

3.1 Implementation of a New NOX Chemistry Option (GRS7) in AERMOD

As discussed in the previous period of performance, UNC-IE developed a new GRS7 chemistry option to AERMOD (version 23132) and compared its performance against AERMOD's existing chemistry options, including Ozone Limiting Method (OLM), Ambient Ratio Method 2 (ARM2), Travel Time Reaction Method (TTRM), Plume Volume Molar Ratio Method (PVMRM), and Generic Reaction Set Method (GRSM), in simulating NO_2 at four core sites (CN, CS, CE, and AQ) in LAX airport during winter (February 1, 2012, to March 13, 2012) and summer (July 18, 2012, to August 28, 2012) episodes. GRS7 is an improved version of AERMOD's beta GRSM chemistry option: GRSM has only two reactions (photolysis of NO_2 to NO and oxidation of NO to NO_2), whereas GRS7 also considers photolysis and oxidation of reactive organic compounds in the NO_x chemistry cycle.

Overall, all chemistry options underestimated observed NO_2; this behavior was attributed mainly to underestimation of NO_x. At the four core monitoring sites, we found that NO_2 prediction was marginally improved in GRS7 over GRSM (mean bias was lowered by 0.1 ppb [3%] in GRS7 over GRSM). Differences between the two chemistry options are largest in the morning hours when background O_3 is low (< 30 ppb) and mean bias was lowered by 1.2 ppb (14%) on average between 07:00 – 09:00 in GRS7. GRSM and GRS7 have identical NO_2 performance in the remaining hours of the day when background O_3 was sufficient; NO_x is low during nighttime when there is lack of photolysis.

As discussed in Venkatram et al. (1998), chemistry age has important implications in determining species' concentration outcomes from chemical reactions. In case of the LAX study, we found that the greater the chemistry age, the more NO_2 concentration is formed from the GRSM and GRS7 chemistry options. Meanwhile, AERMOD limits chemistry age (also known as travel time) of GRSM and TTRM to one hour. As shown in Table 8, we found that at the four core sites (CE, CS, CN and AQ), the median travel times were within one hour but occasionally exceeded this limit. At the monitoring site CE2 (see Figure 2 for location), located southeast about 5.5 km away from LAX, the travel time well exceeded one hour. Since chemical reactions should be estimated in the same time duration it takes for the air mass to travel from source to receptors, it is unreasonable to limit chemistry age to one hour for receptors far away from LAX center, such as CE2.

Our hypothesis is that differences in simulated NO_2 between GRS7 and GRSM were marginal at the four core sites (CE, CN, CS, and AQ) due to their close proximities to emission sources in LAX, and the differences would become larger at receptors farther downwind. Furthermore, if travel time was not limited to one hour, differences between GRSM and GRS7 become even larger, especially at further downwind distances from emissions sources at LAX.

Table 8. Travel time (seconds) from source to selected monitoring stations in Los Angeles International Airport.

Station	Average	Median	95 pct	Max
CE2	5973	5328	12217	17903
CE	1306	966	3503	6593
CS	2602	1891	7530	13069
CN	1321	899	3898	8297
AQ	2753	1726	8064	16062

3.2 Model Configuration

To verify the hypothesis presented above in Section 3.1, UNC-IE utilized the same AERMOD (version 23132) configurations (e.g., plume rise treatment for aircraft emissions and modified meteorological inputs) that were applied in Pandey et al. (2024) and implementation of the GRS7 chemistry option. Emission input data were processed using the FAA's AEDT3e for LAX-related emissions (i.e., aircraft, taxi, gates) and the EDMS emission inventory for LAX for non-aircraft sources. Emissions from aircrafts, taxi segments, and gates were all simulated as AREA sources.

We extended the receptors to a 10 km by 15 km grid spaced 500 km apart and centered on LAX (Figure 21). We modified the AERMOD source code to un-limit travel time, so that chemical reactions were simulated for the same duration as the source-to-receptors travel time.

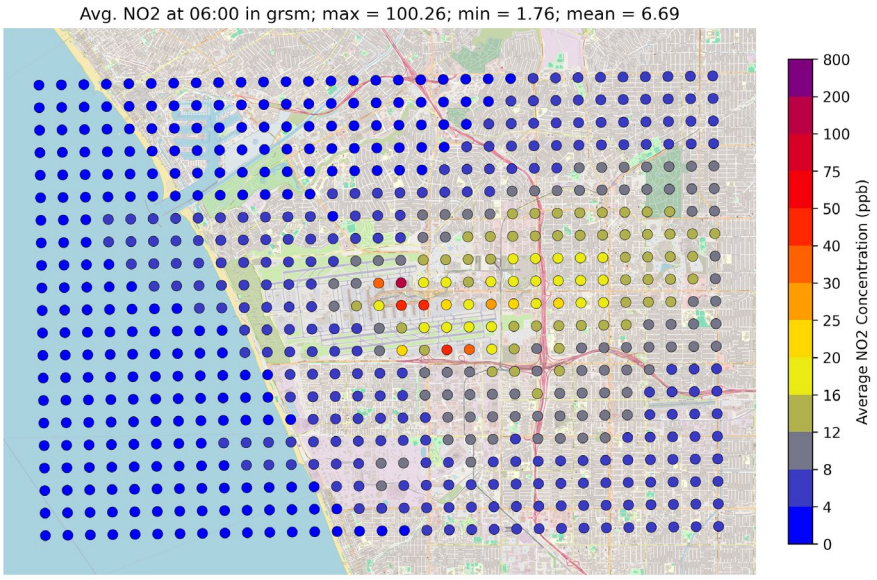

Figure 21. Example of simulated nitrogen dioxide (NO_2) concentrations on the 500 m horizontal resolution receptor grid over Los Angeles International Airport.

3.3 Summary of Findings

Figure 22 shows simulated averaged NO_2 concentrations from GRSM at 6:00 am and 7:00 am local time. Note that this time window is when background O_3 was lowest, thereby increasing the importance of volatile organic compounds (VOC) in GRS7 for the NO-to-NO_2 conversion because O_3 is low. Figure 23 shows differences between the GRS7 and GRSM options,

with the one-hour travel time limitation still in place. We found larger differences between GRS7 and GRSM (up to 5 ppb) at receptors further away from LAX (e.g., receptors on the east side of Interstate I-405). Removing the travel time limitation in GRS7 further enhances the differences between GS7 and GRSM, as shown in Figure 24.

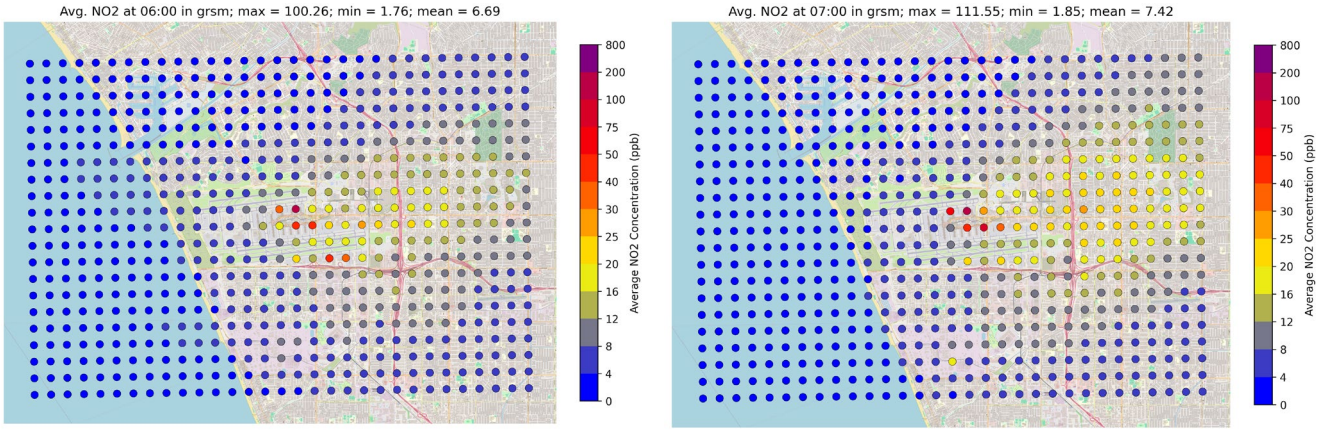

Figure 22. Average nitrogen dioxide (NO_2) concentration as simulated at 6:00 am (left) and 7:00 am (right) local time with the GRSM chemistry option over a 500 m receptor grid. These average concentrations were filtered for hours when wind direction was between 225–315 degrees, which is when AERMOD exhibits the best performance at the four core sites.

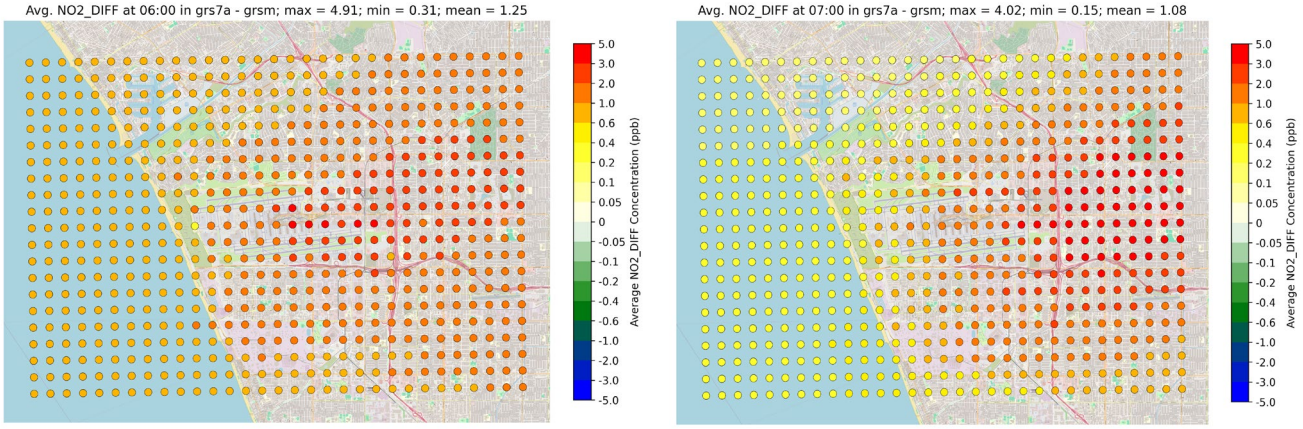

Figure 23. Differences (GRS7 – GRSM) in simulated hourly-average nitrogen dioxide (NO_2) concentrations at 6:00 am (left) and 7:00 am (right) local time over a 500 m receptor grid. Similar to Figure 22, these average concentrations were filtered for hours when wind direction was between 225–315 degrees, which is when AERMOD exhibits the best performance at the four core sites.

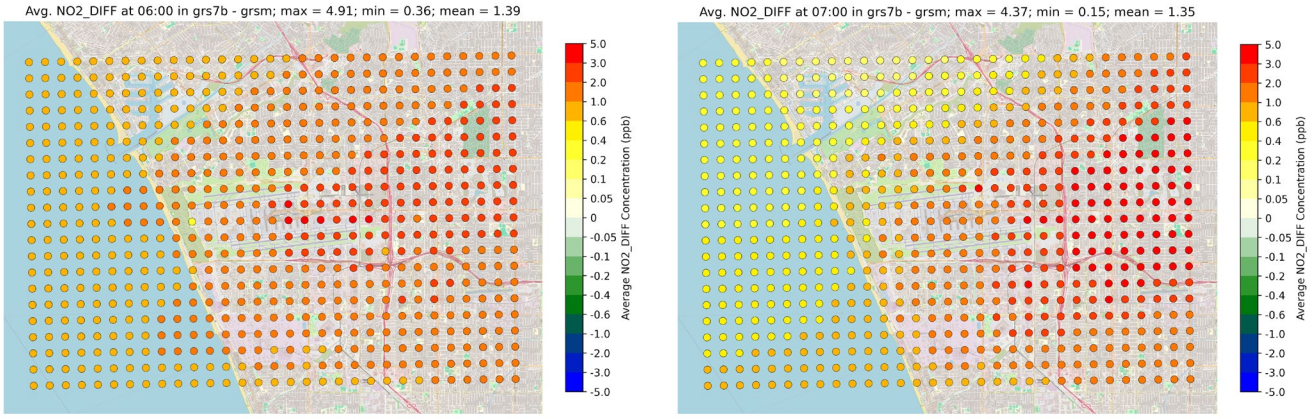

Figure 24. Differences (GRS7 – GRSM) in simulated hourly-average nitrogen dioxide (NO_2) concentrations at 6:00 am (left) and 7:00 am (right) local time over a 500 m receptor grid, with the travel time limitation removed. Similar to Figure 22, these average concentrations were filtered for hours when wind direction was between 225–315 degrees, which is when AERMOD exhibits the best performance at the four core sites.

4. Development of Aircraft Dispersion Model

4.1 Preparing ADM/GADM Emission Inputs

A Python3-based emission processor "AEDT2ADM" was developed to create the emissions input for ADM and GADM. This emission processor's input data files are the AEDT flight segment and performance data. During this period of performance, UNC-IE initiated a substantial update to the AEDT2ADM tool, aiming to significantly expand its capabilities for generating AERMOD-ready input files. Previously limited to polygon-based runway and taxiway ground sources at LAX only, the tool is now being upgraded to support any airport using all gridded sources, including both surface and airborne emissions. The Version 7 update introduces support for VOLUME sources and enables the generation of input files compatible with plume-rise algorithms. To enhance flexibility, the tool is being tested with BOS data to ensure applicability across different airports. Using polygon-based ground source shapes at BOS, UNC-IE successfully created airborne and gridded ground sources. A separate script was developed to summarize segment-level AEDT data, detailing flight counts and emissions by engine type. Comparative analysis of hourly flight activity between BOS (2024) and LAX (2012) revealed discrepancies in BOS data aggregation due to challenges in aggregating segment-level AEDT data to the hourly scale without double counting. This analysis helped UNC-IE refine the process of aggregating and interpreting AEDT segment-level data. Work on Version 7 is ongoing, with a focus not only on evaluating performance at a different airport, but also in evaluating output for VOLUME sources.

4.2 Model Evaluation

This task was on hold during this performance period as our priority was to enhance the aircraft-plume rise algorithm.

Milestones

- Successfully compared AERMOD with plume rise results against the LASPORT dispersion model.
- Extensively analyzed the observation data collected at BOS for the 2024 spring/summer and winter seasons.
- Successfully re-produced the AEDT-generated aircraft emissions for the 2024 spring/summer season for the BOS study.
- Set up the AEDT for the 2024 winter season for the BOS study.

Major Accomplishments

- Successfully updated (using enhanced plume dynamics approach) and implemented the aircraft plume rise algorithm.

Publications

- Published the AREA source meander paper in the *Journal of the Air & Waste Management Association* on October 30, 2024.

Outreach Efforts

- Presented in Alexandria, Virginia, at the ASCENT Fall 2024 meeting on October 29–30, 2024,
- Presented virtually at the ASCENT Spring 2025 meeting on May 14, 2025

Awards

None.

Student Involvement

None.

Plans for Next Period

- Finalize the updated aircraft-plume rise algorithm and optimize the run time.
- Draft a detailed paper on the updated aircraft plume rise algorithm and its evaluation against LAX and BOS data.
- Generate the aircraft emissions inventory using AEDT for the 2024 winter season for the BOS study.
- Perform a detailed AERMOD analysis for the Boston winter study.
- Finalize a detailed paper on GRS7 implementation and evaluation.
- Finalize the ADM and GADM models with all physical and chemical components.

References

Arunachalam, S., Isakov, V., Barzyk, T., Venkatram, A., Weil, J., Naess, B., Valencia, A., Seppanen, C., & Brandmeyer, J. (2017, October 9-12). *C-AIRPORT: a new web-based air quality model for community-scale assessments around airports* [Conference presentation]. 18th International Conference on Harmonization within Atmospheric Dispersion Modelling for Regulatory Purposes, Bologna, Italy.

Arunachalam, S., Valencia, A., Woody, M. C., Snyder, M. G., Huang, J., Weil, J., Soucacos, P., Webb, S., Airport Cooperative Research Program, Transportation Research Board, & National Academies of Sciences, Engineering, and Medicine. (2017). *Dispersion modeling guidance for airports addressing local air quality health concerns*. Transportation Research Board. https://doi.org/10.17226/24881

Barzyk, T. M., Isakov, V., Arunachalam, S., Venkatram, A., Cook, R., & Naess, B. (2015). A near-road modeling system for community-scale assessments of traffic-related air pollution in the United States. *Environmental Modelling & Software, 66*, 46–56. https://doi.org/10.1016/j.envsoft.2014.12.00

Boeing. (2010). *Boeing Projects $700 Billion Commercial Airplanes Market in North America*. Retrieved March 9, 2025, from https://boeing.mediaroom.com/2010-09-02-Boeing-Projects-700-Billion-Commercial-Airplanes-Market-in-North-America

Chowdhury, B., Karamchandani, P. K., Sykes, R. I., Henn, D. S., & Knipping, E. (2015). Reactive puff model SCICHEM: Model enhancements and performance studies. *Atmospheric Environment, 117*, 242–258. https://doi.org/10.1016/j.atmosenv.2015.07.012

Chang, J. C., & Hanna, S. R. (2004). Air quality model performance evaluation. *Meteorology and Atmospheric Physics, 87*(1–3), 167–196. https://doi.org/10.1007/s00703-003-0070-7

Cox, W. M., & Tikvart, J. A. (1990). A statistical procedure for determining the best performing air quality simulation model. *Atmospheric Environment. Part A. General Topics, 24*(9), 2387–2395. https://doi.org/10.1016/0960-1686(90)90331-G

Ross, J., Ahearn, M., Boeker, E., Cumper, J., Downs, R., Goetzinger, S., Gorshkov, S., Malwitz, A., Mittelman, A., Nicholas, B., Reherman, C., Roof, C., Simon, M., Tosa, Y., Wilson, A., DiPardo, J., Majeed, M., Hwang, S., Kuiper, B., & Augustine, S. (2024). *Aviation environmental design tool (AEDT) 3g technical manual*. Federal Aviation Administration. https://www.researchgate.net/publication/386868562_Aviation_Environmental_Design_Tool_AEDT_3g_Technical_Manual

Janicke, U. (2024). Application of Effective Conversion Rates between NO and NO_2 in a Standard Airport Dispersion Model System. *Atmosphere, 15*(5), 574. https://doi.org/10.3390/atmos15050574

Kim, B., Rachami, J., Robinson, D., Robinette, B., Wyle, K. N., Arunachalam, S., Davis, N., Baek, B. H., Shankar, U., Talgo, K.,

Yang, D., Hanna, A. F., Wayson, R. L., Noel, G., Gliff, S. S., Zhao, Y., Hopke, P. K., Kumar, P., Airport Cooperative Research Program, … National Academies of Sciences, Engineering, and Medicine. (2012). *Guidance for quantifying the contribution of airport emissions to local air quality*. Transportation Research Board. https://doi.org/10.17226/22757

Pandey, G., Venkatram, A., & Arunachalam, S. (2022). Evaluating AERMOD with measurements from a major U.S. airport located on a shoreline. *Atmospheric Environment, 294*, 119506. https://doi.org/10.1016/j.atmosenv.2022.119506

Pandey, G., Venkatram, A., & Arunachalam, S. (2023). Accounting for plume rise of aircraft emissions in AERMOD. *Atmospheric Environment, 314*, 120106. https://doi.org/10.1016/j.atmosenv.2023.120106

Pandey, G., Venkatram, A., & Arunachalam, S. (2024). Accounting for plume rise of aircraft emissions and shoreline meteorology enhances AERMOD's description of concentrations measured around Los Angeles airport. *Journal of the Air & Waste Management Association*, 74(10), 726–742. https://doi.org/10.1080/10962247.2024.2394104

Tetra Tech, Inc. (2013). *LAX Air Quality and Source Apportionment Study - Volume 2. Executive Summary*. Los Angeles World Airports.

Valencia, A., Venkatram, A., Heist, D., Carruthers, D., & Arunachalam, S. (2018). Development and Evaluation of the R-LINE Model Algorithms to Account for Chemical Transformation in the Near-road Environment. *Transportation Research. Part D, Transport and Environment, 59*, 464–477. https://doi.org/10.1016/j.trd.2018.01.028

Venkatram, A., Karamchandani, P., Pai, P., & Goldsteins, R. (1994). The development and application of a simplified ozone modeling system (SOMS). *Atmospheric Environment, 28*(22), 3665–3678. https://doi.org/10.1016/1352-2310(94)00190-V

Venkatram, A., Du, S., Hariharan, R., Carter, W., & Goldstein, R. (1998). The concept of species age in photochemical modeling. Atmospheric Environment, 32(20), 3403–3413. https://doi.org/10.1016/S1352-2310(98)00032-6

Wayson, R. L., Fleming, G. G., Noel, G., MacDonald, J., Eberhard, W. L., McCarty, B., Marchbanks, R., et al. (2008). *Lidar Measurement of Exhaust Plume Characteristics from Commercial Jet Turbine Aircraft at The Denver International Airport* (No. FAA-AEE-08-02). U.S. Department of Transportation and NOAA Earth System Research Laboratory. https://rosap.ntl.bts.gov/view/dot/9522/dot_9522_DS1.pdf

Task 2 - Develop and Evaluate a Multiscale WRF-SMOKE-CMAQ Model Application for BOS Focused on UFPs

University of North Carolina at Chapel Hill

Objectives

In this project, our team partnered with ASCENT Project 018 investigators from BU to focus on modeling BOS across various spatial scales. The primary objective was to conduct a thorough intercomparison of measurements and models, with a special emphasis on UFP, mass, and number concentrations resulting from aircraft emissions.

To achieve this goal, we delved into the utilization of two distinct modeling approaches: the CMAQS and Second-order Closure Integrated Puff (SCIPUFF) with SCICHEM models. The SCICHEM model stands out for its integration of comprehensive gas-, aqueous-, and aerosol-phase chemistry within the advanced Gaussian puff model SCIPUFF (Chowdhury, 2015). Noteworthy is its capacity to characterize aircraft impacts with high precision in the immediate vicinity of the source as a series of puffs, thereby offering a significant advancement in the estimation of aircraft-attributable PM compared with previous assessments, notwithstanding its potential large computational times.

It is crucial to highlight that while both CMAQ and SCICHEM share a common aerosol treatment, SCICHEM excels in capturing fine-scale details around the airport. A key outcome of this project is the enhancement of predictions related to aircraft-attributable PM compared with previous estimates. It is worth noting that the use of SCICHEM, which focuses solely on PM mass concentrations, necessitated the development of postprocessing routines. These routines were designed to convert PM mass into a UFP number concentration (UFPNC) using a methodology consistent with CMAQ. Additionally, it is important to mention that, until now, SCICHEM has not been employed to predict UFPNC. This effort introduces a novel avenue of research in our project, showcasing our commitment to develop novel model approaches for source treatment. During this period of performance, our focus has only been on CMAQ, and SCICHEM efforts will be continued later.

In 2017, ASCENT Project 018 investigators made multiple measurements of UFPs at seven locations south and west of BOS. Our team collaborated with BU to obtain these measurements to perform an intercomparison against model outputs.

CMAQ-AEDT Application for Boston Logan International Airport
To complete this task, our team used a nested application of the WRF-SMOKE-CMAQ modeling system, including the AEDT. CMAQ applied to the northern hemisphere at a resolution of 108 km is downscaled to determine the beginning and boundary conditions for the outermost grid, which is set at a resolution of 12 km. The larger-scale conditions are suitably captured for the outermost grid through the nesting down method. From the immediate outer grid, the next 4-km and 1.33-km grids are nested down in accordance with typical modeling procedures. A transition and improvement of atmospheric conditions are made by this nested technique, which permits a more accurate and thorough depiction of the dynamics as spatial resolution increases. We used the following to develop this application:

- Meteorology from Modern-Era Retrospective analysis for Research and Applications (MERRA) (Rienecker et al., 2011) downscaled with WRF v3.8 (Skamarock et al., 2008)
- Background emissions from NEI processed through SMOKE v3.6 (Baek & Seppanen, 2018)
- Aircraft emissions for the 2017 BOS study from the AEDT processed through AEDT Proc (Baek et al., 2012)
- CMAQ v5.33 enhanced with the new aircraft-specific emissions module (Appel et al., 2021)

Development of Aircraft Emission Inventory for Boston Logan International Airport by using AEDT
The TT is derived solely from radar surveillance sources. One of the primary data feeds to the Center for Advanced Aviation System Development (CAASD) is the National Offload Program (NOP) which provides coverage at 158 Terminal Radar Approach Control (TRACON) and 20 Air Route Traffic Control Centers (ARTCC). The ARTCC facilities provide a post-processed set of Common Message Set (CMS) data, whereas the TRACON facilities come directly from Standard Terminal Automation Replacement System (STARS) or Automated Radar Terminal System (ARTS) facilities, each reporting a separate post-processed data format (108 ARTS facilities and 50 STARS facilities). Both ARTCC and STARS facilities compute multi-sensor fused reports, whereas the ARTS facilities provide individual radar sensor reports. ARTCC data have the largest spatial coverage per facility, with a high-quality flight plan and metadata reported at 12 second updates. TRACON facilities have higher fidelity position measurements reported at roughly 4 second updates but are generally limited in this coverage to about 60 nautical miles (NM) of the airport and contain sparser flight metadata.

TT flight operation data have information about each aircraft operation (e.g., aircraft type, airport, runway, and time of arrival and departure, etc.) and has detailed information about each aircraft operation with real-time tracking, including time, latitude, longitude, and altitude. Our main goal is to enhance our modeling simulation to encompass a whole month of January and July 2017, with TT by using the AEDT. Our team utilized AEDT version 3g to create a BOS-specific emission inventory that corresponds with the BU's UFP measurement campaign's duration. Using real-time aircraft operation data to create emissions guarantees more precise calculation of the emissions in the airport vicinity across the designated time frame, compared to other emissions inventories.

Comparison of Boston Logan International Airport Emissions with Different Aircraft Emission Inventories
EPA provides aircraft emissions estimates in the NEI as a point source for all airports in the U.S. Thus, for BOS, our team has aircraft emissions during LTO assigned to a single latitude/longitude. While NEI emission inventory provides us with a starting point for use in CMAQ, two different approaches for emission creation were explored to better understand aircraft impact on air quality.

- The emission scenarios considered in this study are:
  - NoBOS: Background emission inventory based on NEI 2017 by excluding BOS
  - AEDT2d-2017-N: 2017 NEI based emissions inventory for BOS, generated using AEDT version 2d
  - AEDT2d-2017-S: 2017 global straight line segment data provided by Volpe for BOS, generated using AEDT version 2d
  - AEDT3g-2017-T: 2017 Thread Track flight operations data by MITRE, generated using AEDT version 3g

Besides improvement in spatial allocation in developing emissions estimates, treatment of particle size distribution was also refined in CMAQ as follows:

- Aircraft Specific Aerosol Size Distribution (ASASD) was applied only for BOS emissions in this study:
  - Geometric Mean Diameter (GMD): 60 nm - 23.2 nm (Moore et al., 2017)
  - Geometric Standard Deviation (GSD): 1.7 nm - 1.56 nm (Moore et al., 2017)
  - Both Geometric Mean Diameter and Standard Deviation (GMDSD) changed as above

Assessment of Ultrafine Particles through Field Observations
The ASCENT Project 018 team at BU made field observations of UFPNC in 2017 at seven fixed sites along the aircraft arrival and departure pathways, near BOS in Figure 25. These monitoring stations were selected because of the varying distances

and UFPNC contributions from BOS. The only one in the northern part of the airport is Chelsea (CHE). Two of the monitoring stations in the southern regions (N1 and N2) are the closest to the airport. Two intermediate sites (I1 and I2) are in the middle, and the last two monitoring stations (far sites F1 and F2) are the furthest distance. UFPNC measurement data were collected from January to September 2017.

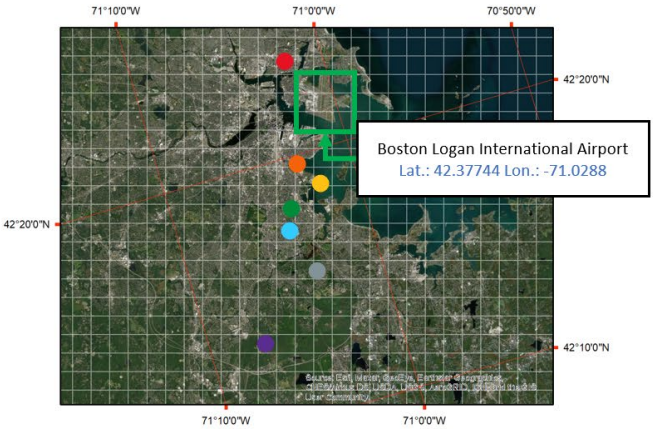

Location	Distance (km)	Color
Airport	-	Green Box
CHE	4	Red
N1	3	Orange
N2	4	Yellow
I1	7	Green
I2	9	Light Blue
F1	12	Gray
F2	17	Purple

Figure 25. CMAQ-based modeling at high resolution 1.33 km by 1.33 km with location of seven monitoring sites near Boston Logan International Airport. CHE: Chelsea.

Research Approach

CMAQ-AEDT Application for Boston Logan International Airport

UFP concentrations at BOS were simulated using the WRF-SMOKE-CMAQ modeling framework in Figure 26. The WRF model was used to create meteorological data. The sigma vertical coordinate system, with 35 vertical layers that reach up to 50 hPa (lowest layer of approximately 10 to 20 m above ground level), was used for this work.

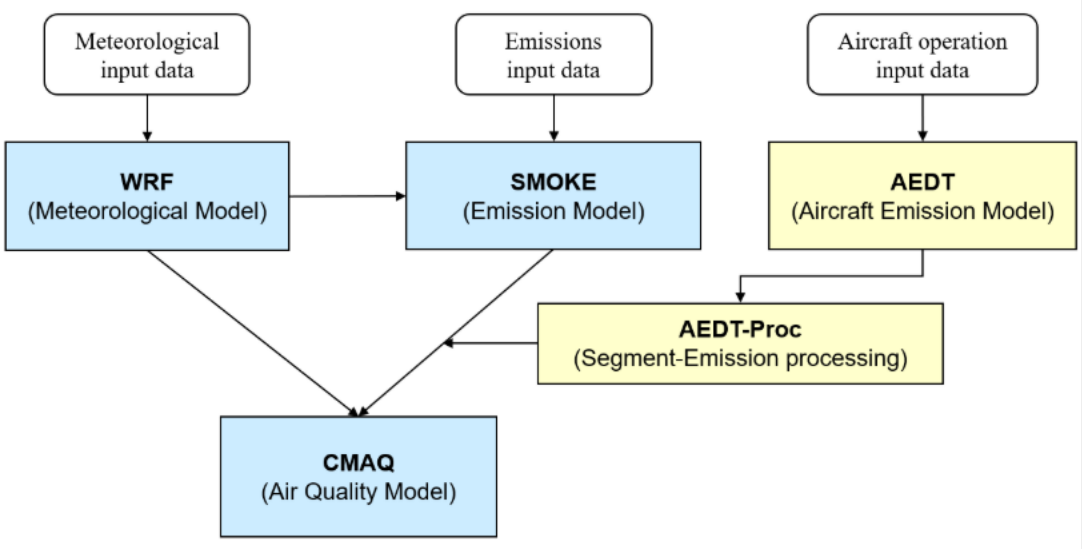

Figure 26. CMAQ application schematic for Boston Logan International Airport with Aviation Environmental Design Tool (AEDT). CMAQ: Community Multiscale Air Quality, SMOKE: Sparse Matrix Operator Kernel Emissions, WRF: Weather Research and Forecasting.

Background emissions were generated based on the 2017 NEI using the SMOKE processing system, except for emissions that came from BOS by using AEDT2d-2017-N. The particle mass concentration was computed using CMAQ configured with the aerosol module version 6 (AERO6) for the aerosol chemistry and the revision 3 of the Carbon Bond 6 mechanism (CB6r3) for the gas-phase chemistry. CMAQ converts particle mass concentration into Particle Number Concentration (PNC) using particle diameter, particle size distribution, and assumed particle density information (Binkowski & Roselle, 2003). PNC is estimated by CMAQ for the entire mass and thus one cannot distinguish between non-volatile particulate matter (nvPM) and volatile particulate matter (vPM) components for the concentrations predicted by CMAQ. Per Equations 5 and 6, our team used a number of parameters for Aitken mode (i) and accumulation mode (j) for total particle number ($N_{i,j}$), particle geometric diameter ($D_{g\,i,j}$), particle geometric standard deviation ($\sigma_{g\,i,j}$), upper diameter cut (UDC), and lower diameter cut (LDC), using the error function (ERF) (Jiang et al., 2006; Meng & Seinfeld, 1994) approach for the concentration of UFPNC. LDC was set at 0.07 µm due to the instrument's low detection limit (LDL) and defined UDC at 0.1 µm, consistent with the UFP definition (Hughes et al., 1998). Our team used a 15-day spin-up period from June 16 to June 30 for the month of July 2017. Initial and boundary conditions were based on the 108-km Northern Hemisphere domain ("108NHEMI").

$$UFP\ number\ for\ Aitken\ mode\ =\ \frac{N_i}{2}\left[1+ERF\left(\frac{lnln\left(\frac{UDC}{D_i}\right)}{\sqrt{2}ln\sigma_i}\right)\right]\ -\ \frac{N_i}{2}\left[1+ERF\left(\frac{lnln\left(\frac{LDC}{D_i}\right)}{\sqrt{2}ln\sigma_i}\right)\right] \quad \text{(Eq. 5)}$$

$$UFP\ number\ for\ accumulation\ mode\ =\ \frac{N_j}{2}\left[1+ERF\left(\frac{lnln\left(\frac{UDC}{D_j}\right)}{\sqrt{2}ln\sigma_j}\right)\right]\ -\ \frac{N_j}{2}\left[1+ERF\left(\frac{lnln\left(\frac{LDC}{D_j}\right)}{\sqrt{2}ln\sigma_j}\right)\right] \quad \text{(Eq. 6)}$$

Our team modeled CMAQ with 35 layers and horizontal resolutions of 12 km, 4 km, and 1.33 km for the study period. Apart from the Aircraft Emission Inventories (AEI) for BOS, all simulations used the same default CMAQ parameters, except aircraft-specific aerosol size distribution.

Development of AEDT Emission Inventory for Boston Logan International Airport by UNC-IE

The key differences among these inventories are in how the segments are spatially and temporally distributed. In AEDT2d-2017-N, aircraft LTO emissions are lumped into the surface layer at a few coordinates based on aircraft type, with a uniform temporal profile for all airports. In contrast, both AEDT2d-2017-S and AEDT3g-2017-T distribute emissions along flight paths with hourly temporal resolution. AEDT2d-2017-S simplifies segments as straight-line paths centered on the airport, illustrating that emissions spread over regions where no runways exist due to the generalized representation of departure and arrival paths. On the other hand, AEDT3g-2017-T confines emissions to the actual corridors of aircraft movement along runways at BOS, yielding emissions in the correct places.

For example, Figure 27 provides the NEI-based spatial mapping and a snapshot (July 3, 2017, at 09:00 EST) of spatial allocation for the straight-segment and TT operations. In the AEDT2d-2017-N (green markers), emissions are assigned to only two grid cells at the airport property and treated as point sources. AEDT2d-2017-S (red) disperses emissions along straight routes radiating from the airport's center, while AEDT3g-2017-T (blue) follows the actual flight trajectories aligned with runways. This underscores that the 3-dimensional (3D) AEI (especially AEDT3g-2017-T) captures the spatial pattern of emissions more realistically than the 2-dimensional (2D) AEI.

Figure 27. Spatial allocation differences among AEDT2d-2017-N (no temporal information) (green), AEDT2d-2017-S (red), and AEDT3g-2017-T (blue) on July 3, 2017, at 9:00 AM (1.33 km × 1.33 km grid).

Comparison of Boston Logan International Airport Emissions with Different Air Emissions Inventories

Our team compared the monthly total mass of major pollutants from the three BOS AEIs to calculate how the choice of emissions model affects the overall emission quantities. In Table 9, we summarize the total emissions for AEDT2d-2017-N (NEI-based), AEDT2d-2017-S (segment-based), and AEDT3g-2017-T (TT-based) for both January and July. The pollutants include the nvPM, volatile fuel organics (PMFO), volatile sulfate PM (PMSO), hydrocarbon (HC), NO_x, SO_2, and carbon monoxide (CO).

For January 2017, nvPM shows the highest (0.66 short tons) with AEDT2d-2017-N; others were between 0.40–0.42 short tons. AEDT3g-2017-T exhibited the highest PMFO among AEIs, while AEDT2d-2017-S was lower than AEDT3g-2017-T and AEDT2d-2017-N. PMSO, which is derived from SO_2 via assumed conversion rates in AEDT, is the highest in AEDT3g-2017-T, even though SO_2 shows the highest in AEDT2d-2017-N, suggesting AEDT2d-2017-N might use a lower conversion rate value in AEDT version 2d. Three AEIs show different magnitudes within PM components.

HC and CO remain the highest with AEDT2d-2017-N. NO_x is the only pollutant which is similar across all three AEIs (102–115 short tons). AEDT3g-2017-T aligns with AEDT2d-2017-N for PMFO, NO_x, SO_2, and CO. AEDT2d-2017-S had the lowest emissions in most categories due to fewer flight numbers than AEDT3g-2017-T.

Table 9. Monthly total aircraft emissions inventories (short tons/year) in January (Jan) and July (Jul) for non-volatile particulate matter (nvPM), volatile fuel organics (PMFO), volatile sulfate PM (PMSO), Hydrocarbon (HC), (Nitrogen oxides (NO_x), sulfur dioxides (SO_2), and carbon monoxide (CO).

Month	AEI	nvPM	PMFO	PMSO	HC	NO_x	SO_2	CO
Jan	AEDT2d-2017-N	0.66	0.36	0.13	28.54	102.19	14.16	231.98
	AEDT2d-2017-S	0.40	0.08	0.31	6.10	115.23	8.37	76.38
	AEDT3g-2017-T	0.42	0.40	0.50	15.67	113.12	13.67	205.39
Jul	AEDT2d-2017-N	0.82	0.45	0.16	35.67	127.74	17.69	289.97
	AEDT2d-2017-S	0.50	0.11	0.41	8.78	150.03	11.34	112.54
	AEDT3g-2017-T	0.53	0.51	0.62	21.01	142.88	16.88	281.13

The pattern of pollutants in July 2017 is broadly similar to January, though absolute amounts are slightly different, reflecting seasonal differences in number of operations, not meteorology. For nvPM, AEDT2d-2017-N is 0.82 short tons, whereas both AEDT3g-2017-T (0.53 short tons) and AEDT2d-2017-S (0.50 short tons) are lower. For PMFO, AEDT3g-2017-T is the highest, and AEDT2d-2017-S is the lowest. PMSO is also the highest in AEDT3g-2017-T, followed by AEDT2d-2017-S and AEDT2d-2017-N. For the gaseous pollutants in July, AEDT2d-2017-N stands out with the highest HC, SO_2, and CO emissions among the three. For NO_x emissions, all AEIs are relatively similar (around 127–150 short tons) for July, as in January. Overall, emissions in July suggest that the AEDT2d-2017-S inventory underestimates emissions for almost all pollutants (except NO_x). The AEDT2d-2017-N and AEDT3g-2017-T can either overestimate or underestimate AEIs for some pollutants. Understanding AEI discrepancies is important because these will influence the modeled UFP.

Assessment of Ultrafine Particles through Field Observations

Figure 28 presents diurnal variation of observed UFPNC and modeled UFPNC with seven modeling scenarios (NoBOS, AEDT2d-2017-N Base/GMDSD, AEDT2d-2017-S Base/GMDSD, and AEDT3g-2017-T Base/GMDSD) at seven measurements near BOS. The top subplots at each site show the UFPNC diurnal variation, and the bottom subplots indicate the diurnal BOS contribution to UFPNC by AEIs compared to NoBOS.

At CHE, the only monitoring station located northwest of BOS (4km), the observations show UFPNC spikes during rush hour at 7:00 AM and 8:00 PM. All modeled scenarios were able to reproduce the diurnal shape, but all overestimated observed UFPNC in the morning (5-10 h) and nighttime (21-5 h) and underestimated observed UFPNC in the evening (18-21 h). The BOS contribution fraction in GMDSD scenarios reaches around 5–20% at 8:00 to 9:00 PM at CHE.

At N1, the observed UFPNC is higher than 8,000 #/cm³ throughout the daytime, but modeled UFPNC underestimated during the daytime, except in the early morning. The AEDT3g-2017-T GMDSD scenario only shows noticeable diurnal contribution to UFPNC at 5:00 AM (10%) and 9:00 PM (10%). N2 shows similar observed UFPNC and modeled UFPNC diurnal variations. At I1 and I2, observed UFPNC reaches 20,000 and 15,000 #/cm³, respectively, around 7:00 to 8:00 PM, which might be a result of the I-93 highway. The modeled BOS contribution to UFPNC in GMDSD scenarios dropped to 3–4% during the morning peak at I1 and I2.

At F1, CMAQ was able to reproduce the UFPNC diurnal shape, even though modeled UFPNC underestimates the observed UFPNC, but the BOS contribution to UFPNC in AEDT3g-2017-T was about 2%. The maximum BOS contribution at F2 was around 0.3%, indicating the dilution of AEs at a farther distance. Figure 28 demonstrates that CMAQ underestimates the magnitude of observed UFPNC, except at CHE. CMAQ with the GMDSD scenario captures the spatial gradient in airport influence (highest at the nearest sites, moderate at the intermediate sites, and negligible at the farthest sites) and calculates the contribution of an aviation source that cannot be distinguished from other sources in observation.

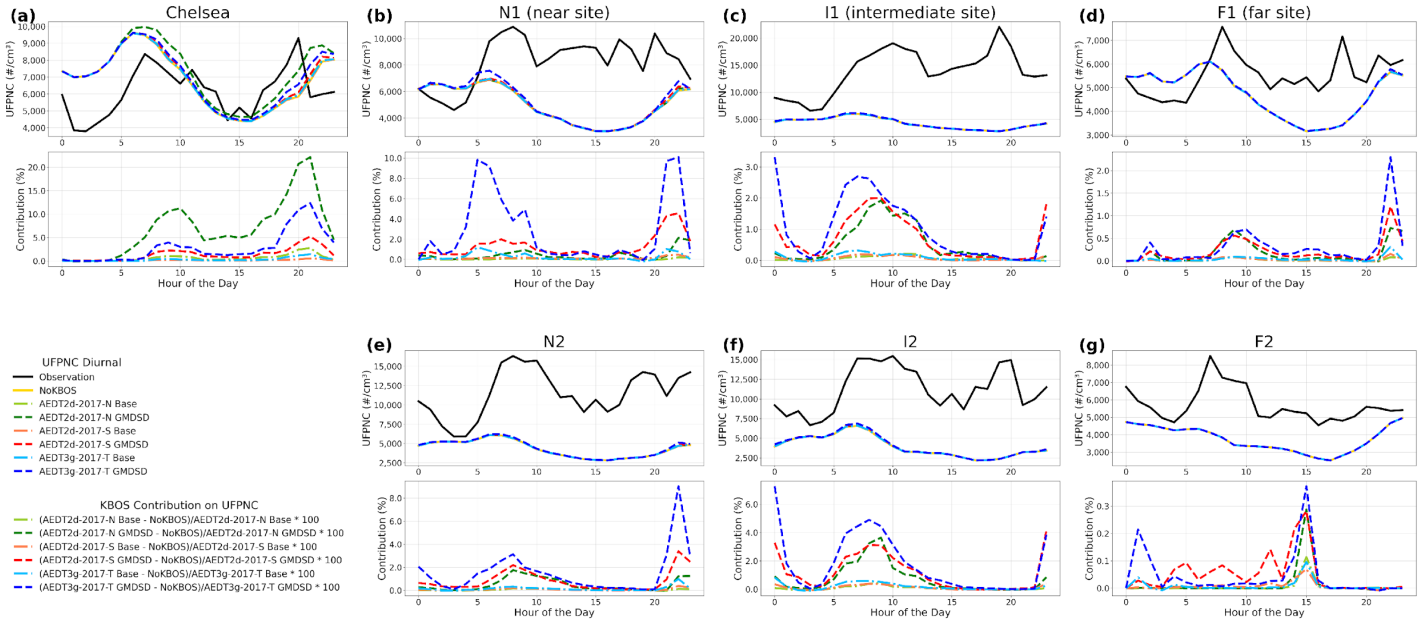

Figure 28. Diurnal variation of ultrafine particles number concentration (UFPNC) (top subplots) and diurnal BOS contribution to UFPNC (bottom subplots) at seven monitoring stations (CHE [Chelsea], near sites [N1 and N2], intermediate sites [I1 and I2], and far sites [F1 and F2]) with observations and seven scenarios.

Milestones

- Completed the development of 3D BOS inventories with TT flight operations using the AEDT for January and July 2017 and repeated CMAQ simulations.
- Completed a comprehensive draft of a paper exploring UFPNC at BOS, and it is currently undergoing thorough review by the co-authors.

Major Accomplishments

- Use TT data for BOS to create our own airport-level inventory, gaining AEDT track creation skills and a further understanding of aircraft operation data in running the AEDT.

Publications

None.

Outreach Efforts

- Hyeongseok (Darby) Kim presented a poster, "Measurement and Modeled Ultrafine Particles from Aircraft Landing and Takeoff Operations at Boston Logan Airport (KBOS)," at the 23rd Annual CMAS Conference, held in Chapel Hill, North Carolina, on October 21–23, 2024.

Awards

None.

Student Involvement

Hyeongseok (Darby) Kim is a PhD student involved in this task performing CMAQ simulations and AEDT modeling.

Plans for Next Period

- Finalize the BOS UFPNC paper and submit it to a peer-reviewed journal.

References

Appel, K. W., Bash, J. O., Fahey, K. M., Foley, K. M., Gilliam, R. C., Hogrefe, C., Hutzell, W. T., Kang, D., Mathur, R., Murphy, B. N., Napelenok, S. L., Nolte, C. G., Pleim, J. E., Pouliot, G. A., Pye, H. O. T., Ran, L., Roselle, S. J., Sarwar, G., Schwede, D. B., . . . Wong, D. C. (2021). The Community Multiscale Air Quality (CMAQ) model versions 5.3 and 5.3.1: System updates and evaluation. *Geoscientific. Model Development, 14*(5), 2867–2897. https://doi.org/10.5194/gmd-14-2867-2021

Baek, B. H., Arunachalam, S., Woody, M., Vennam, P. L., Omary, M., Binkowski, F., & Fleming, G. (2012, October 15-17). *A new interface to model global commercial aircraft emissions from the FAA Aviation Environmental Design Tool (AEDT) in air quality models* [Conference presentation]. 11th Annual CMAS Conference, Chapel Hill, North Carolina.

Baek, B. H., & Seppanen, C. (2018). *Sparse Matrix Operator Kernel Emissions (SMOKE) modeling system*. Zenodo. https://doi.org/10.5281/zenodo.1421403

Binkowski, F. S., & Roselle, S. J. (2003). Models-3 Community Multiscale Air Quality (CMAQ) model aerosol component 1. Model description. *Journal of Geophysical Research: Atmospheres, 108*(D6). https://doi.org/10.1029/2001JD001409

Chowdhury, B. (2015). Reactive puff model SCICHEM: Model enhancements and performance studies. *Atmospheric Environment*, 117, 242-258. https://doi.org/10.1016/j.atmosenv.2015.07.012

Hughes, L. S., Cass, G. R., Gone, J., Ames, M., & Olmez, I. (1998). Physical and chemical characterization of atmospheric ultrafine particles in the Los Angeles area. *Environmental Science & Technology*, 32(9), 1153–61. https://doi.org/10.1021/es970280r

Jiang, W., Smyth, S., Giroux, E., Roth, H., & Yin, D. (2006). Differences between CMAQ fine mode particle and $PM_{2.5}$ concentrations and their impact on model performance evaluation in the Lower Fraser Valley. *Atmospheric Environment*, 40(26), 4973–85. https://doi.org/10.1016/j.atmosenv.2005.10.069

Meng, Z., & Seinfeld, J. H. (1994). On the source of the submicrometer droplet mode of urban and regional aerosols. *Aerosol Science and Technology*, 20(3). 253–65. https://doi.org/10.1080/02786829408959681

Moore, R. H., Shook, M. A., Ziemba, L. D., DiGangi, J. P., Winstead, E. L., Rauch, B., Jurkat, T., Thornhill, K. L., Crosbie, E. C., Robinson, C., Shingler, T. J., Anderson, B. E. (2017). Take-off engine particle emission indices for in-service aircraft at Los Angeles International Airport. *Scientific Data, 4*(1), 170198. https://doi.org/10.1038/sdata.2017.198

Rienecker, M. M., Suarez, M. J., Gelaro, R., Todling, R., Bacmeister, J., Liu, E., Bosilovich, M. G., Schubert, S. D., Takacs, L., Kim, G., Bloom, S., Chen, J., Collins, D., Conaty, A., da Silva, A., Gu, W., Joiner, J., Koster, R. D., Lucchesi, R., . . . Woollen, J. (2011). MERRA: NASA's modern-era retrospective analysis for research and applications. *Journal of Climate*, 24(14), 3624-3648. https://doi.org/10.1175/JCLI-D-11-00015.1

Skamarock, W. C., Klemp, J., Dudhia, J., Gill, D. O., Barker, D., Wang, W., & Powers, J. G. (2008). *A description of the advanced research WRF version 3*. University Corporation for Atmospheric Research. https://doi.org/10.5065/D68S4MVH

Task 3 - Implement Volatile Particulate Matter Plume-Scale Modeling into a Community Multiscale Air Quality Application

University of North Carolina at Chapel Hill

Objectives

In previous work, UNC-IE accounted for the formation of non-traditional secondary organic aerosols (SOA) from the oxidation of semi-volatile organic compounds (SVOC) and intermediate-volatility organic compounds (IVOC) emitted from aircraft, and we utilized alternative emission estimates from the Aerosol Dynamics Simulation Code (ADSC). ADSC is a one-dimensional, plume-scale model that estimates engine-specific PM emissions and the emission of SVOCs and IVOCs under ambient conditions, accounting for relative humidity (RH) and temperature. To extend this work, ADSC for a vPM has been developed by Aerodyne. This model uses the vPM modeling tool developed and enhanced by National Aeronautics and Space Administration (NASA). FAA used ADSC for a parametric analysis of vPM to provide an additional physical perspective on vPM properties and evolution for quantities that are difficult to measure directly or continuously. This is because the engine exit plane is too hot for the condensable species to be in the particle phase, so only the nvPM particles are present at the exit plane.

The parametric set of vPM modeling studies usually spans the range of experimental conditions that have been measured or may be measured in the foreseeable future. These studies also enable an assessment of impacts on vPM properties, such as size and composition due to changes in fuel sulfur contents (FSC) and on fuel HC levels and composition. The interactions between these changes in condensable species and existing soot particles are tracked as a function of FSC, HC concentrations, HC profiles, and concentrations modeled at some distance from downstream (e.g., 0 m to 1000 m) (Wong, 2015). We propose to take advantage of this parameterization and extend previous work by Woody et al. (2016) and Jones and Miake-Lye (2024) to obtain vPM emission indices (EIs) to calculate vPM emissions considering vPM parameters for an airport-level air quality study. We hypothesize that this capability will enable accurate characterization of $PM_{2.5}$ formation at local scales in the immediate vicinity of the airport and enhance air quality health impact studies. With resources permitting, we will develop this application for a single airport next year and apply to airports nationwide with a more recent emission inventory.

Research Approach

Research on Aerosol Dynamics Simulation Code

UNC-IE reviewed previous ADSC modeling work and explored the optimal CMAQ configuration to be used given recent advances in CMAQ version 5.5. We also established contact with Aerodyne to obtain the latest version of the ADSC with vPM treatment to get EIs to calculate aircraft emission for vPM. We obtained the ADSC and ran a series of tests to ensure that we can benchmark the model. After obtaining initial benchmarking results, we ran the model for multiple combinations of engines and atmospheric conditions to create a lookup table for use in CMAQ, and we can also use the EI values from Aerodyne's study. We have worked closely with Aerodyne to document model issues as they come up for future references and updates.

1) **ADSC Modeling Work for vPM**
   - The new parametrization for vPM modeling will be completed, particularly for PMSO and PMFO. The new vPM approach would use EI_{PMFO} and EI_{PMSO}, generated by ADSC. The EI will be multiplied by the fuel burn from AEDT results to calculate aircraft emissions. FSC was also chosen to span a range of values that are representative of those found in aviation fuel.
     - Less than 5-15 ppm FSC to be representative of sustainable aviation fuel (SAF) or the ND-MAX/ECLIF2 campaign's fuels (Schripp et al., 2022)
     - 680 ppm FSC (0.068 weight percent) based on Doc 9889, Airport Air Quality Manual, Second Edition, 2020 from ICAO (ICAO, 2020)

2) **CMAQ Application of vPM for BOS**
   - For this assignment, we adapted the same WRF-SMOKE-CMAQ modeling system methodology from Task 2, but we added ADSC to calculate vPM emissions for aircraft before processing through AEDT-Proc by multiplying fuel burn rate from AEDT output (Figure 29).

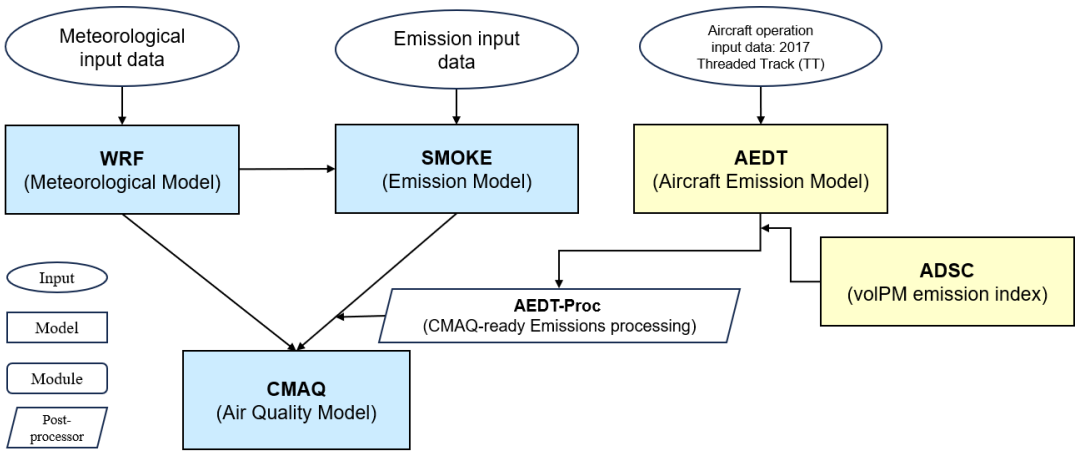

Figure 29. Community Multiscale Air Quality (CMAQ) application schematic for Boston Logan International Airport with Aerosol Dynamics Simulation Code (ADSC) and Aviation Environmental Design Tool (AEDT). SMOKE: Sparse Matrix Operator Kernel Emissions, WRF: Weather Research and Forecasting.

3) **Contribution of vPM on SOA and UFPNC**
   - For this application, the emission inventories pertaining to non-aviation sectors draw upon data provided by the EPA's NEI for 2017, which are projected from NEI 2016. To enhance our vPM emissions for aircraft, we aim to procure BOS-specific airport-level emission inventories for the year 2017 directly from AEDT through TT operations. Also, the AEDT fuel burn results will be extracted and multiplied with the EIs from ADSC for vPM to calculate aircraft emissions. The following emissions scenarios are considered:
     i. BOS emissions in NEI 2017 (based on AEDT) during LTO cycles
     ii. BOS emissions exported by AEDT version 3g during LTO cycles for 2017
     iii. BOS emissions generated by Fuel Burn from AEDT with EI_{PMSO} and EI_{PMFO} from ADSC
   - Seasonal changes in vPM play a central role in understanding aircraft-related air quality impacts, and this work explores how SOA and UFP seasonal patterns shift when vPM emissions are recalculated using specific particle size bins (e.g., Aitken mode [0–20 nm] and accumulation mode [20–100 nm]). Our team also examines how FSC influences particulate mass, number, and the evolving size distribution within CMAQ, providing a more complete view of how PM nucleates and condenses as they mix and dilute in the atmosphere after being emitted from aircraft. We will assess how SAF alters the contribution of vPM, offering insights into the benefits of SAF from an air quality perspective.

Milestones
None.

Major Accomplishments
- Obtained ADSC with vPM treatment from Aerodyne and installed and ran the model to create a new lookup table for use in CMAQ.

Publications
None.

Outreach Efforts
None.

Awards
None.

Student Involvement

Hyeongseok (Darby) Kim is a PhD student involved in this task performing ADSC-CMAQ modeling.

Plans for Next Period

- Create flight operations as an AEDT input data format and run the AEDT for BOS for January and July 2017.
- Run ADSC and create vPM emissions by multiplying AEDT results.
- Conduct CMAQ modeling using the new vPM emissions.

References

ICAO. (2020). *Airport Air Quality Manual* (Doc 9889). International Civil Aviation Organization. https://store.icao.int/en/airport-air-quality-manual-doc-9889

Jones, S. H., & Miake-Lye, R. C. (2024). Parameterization of H_2SO_4 and organic contributions to volatile PM in aircraft plumes at ground idle. *Journal of the Air & Waste Management Association, 74*(7), 490-510. https://doi.org/10.1080/10962247.2024.2354820

Schripp, T., Anderson, B. E., Bauder, U., Rauch, B., Corbin, J. C., Smallwood, G. J., Lobo, P., Crosbie, E. C., Shook, M. A., Miake-Lye, R. C., Yu, Z., Freedman, A., Whitefield, P. D., Robinson, C. E., Achterberg, S. L., Köhler, M., Oßwald, P., Grein, T., Sauer, D., LeClercq, P. (2022). Aircraft engine particulate matter emissions from sustainable aviation fuels: Results from ground-based measurements during the NASA/DLR campaign ECLIF2/ND-MAX. *Fuel, 325*, 124764. https://doi.org/10.1016/j.fuel.2022.124764

Wong, H.-W. (2015). Roles of Organic Emissions in the Formation of Near Field Aircraft-Emitted Volatile Particulate Matter: A Kinetic Microphysical Modeling Study. *Journal of Engineering for Gas Turbines and Power, 137*(7). https://doi.org/10.1115/1.4029366

Woody, M., Wong, H.-W., West, J. J., & Arunachalam, S. (2016). Multiscale predictions of aviation-attributable $PM_{2.5}$ for U.S. airports modeled using CMAQ with plume-in-grid and an aircraft-specific 1-D emission model. *Atmospheric Environment, 147*, 384-394. http://dx.doi.org/10.1016/j.atmosenv.2016.10.016